OPTICAL CHARACTERIZATION OF ON-CHIP SILICON NITRIDE MICRORESONATORS

A Dissertation

Submitted to the Faculty

of

Purdue University

by

Abdullah Al Noman

In Partial Fulfillment of the

Requirements for the Degree

of

Master of Science in Electrical and Computer Engineering

May 2016

Purdue University

West Lafayette, Indiana

I want to dedicate this thesis to

My Mother,

Who is watching me from heaven

ACKNOWLEDGMENTS

Firstly I want to convey my gratitude to Almighty for giving me the ability and strength to complete this thesis. I want to convey my thanks and gratitude to my supervisor Professor Andrew M Weiner. It was impossible for me to finish this thesis without his continuous support and guidance. Also, I went through a few difficult situations in last couple of years and he has supported me with everything. I am thankful to Professor Minghao Qi for his collaboration with our group along with some valuable discussions and encouragements. I am also grateful to my committee members Professor Peter Bermel and Professor Alexandra Boltasseva for their valuable time and help.

I am grateful to our lab manager Dr. Daniel E. Leaird for his help and guidance. Whenever I faced any problem, he was always there to solve it. I'm ever grateful to our wonderful group members for their help and support from the beginning. I want to specially mention Dr. Xiaoxiao Xue, Dr. Pei Hsun Wang and Cong Wang's name, they have been extremely patient and helpful and have been instrumental in developing my skills and knowledge in this area. I'm also grateful to Jose Jaramillo and Steven Chen for their extensive support and help. I am grateful to our collaborator Professor Minghao Qi's group, specially Dr. Yi Xuan and Kyunghun Han who fabricated all the chips for our measurements and Dr. Sangsik Kim for his valuable advice and discussions.

Finally I'm grateful to my family members and my friends whose constant support and encouragement has been very very important for my life.

TABLE OF CONTENTS

Page

LIST OF TABLES

LIST OF FIGURES

Figure Page

Figure Page

SYMBOLS

c	Velocity of Light
v_g	Group Velocity
ϵ	Electric Permeability
μ	Magnetic Permittivity
ω	Angular Frequency
λ	Wavelength of Light
β	Propagation Constant
ψ	Spectral Phase
β_2	Second Order Dispersion
D	Dispersion Coefficient
T	Transmittance
n_2	Kerr Non-linearity
f_{CEO}	Carrier Envelope Offset Frequency
κ	Coupling Coefficient
Q	Quality Factor
n_g	Group Refractive Index

ABBREVIATIONS

abbr	abbreviation
SiN	Silicon Nitride
FSR	Free Spectral Range
BPF	Band Pass Filter
LPF	Low Pass Filter
PC	Polarization Controller
PD	Photo Diode
DL	Diode Laser
Q-factor	Quality Factor
IR	Infra Red
GVD	Group Velocity Dispersion
GDD	Group Delay Dispersion
ER	Extinction Ratio
FWHM	Full Width at Half Maximum
OSA	Optical Spectrum Analyzer
ESA	Electrical Spectrum Analyzer
FWM	Four Wave Mixing
MPB	MIT Photonic Bands

ABSTRACT

Al Noman, Abdullah M.S.E.C.E., Purdue University, May 2016. Optical Characterization of On-Chip Silicon Nitride Microresonators. Major Professor: Andrew M. Weiner.

Optical Characterization of on-chip microresonators is very important in microresonator research area. Full optical characterization includes both the time and the frequency domain characterizations by which we can get some basic parameters and properties like Free Spectral range (FSR), Quality Factor, Dispersion, ability to generate coherent Frequency Comb etc. These parameters and properties are very important because a lot of applications of microring resonators depend on the value of those parameters that we obtain from optical characterizations. In this thesis, we tried to describe some of the fundamental frequency domain characterization methods namely the Transmission Spectrum measurement, Quality factor measurement, Dispersion measurement and Optical Frequency Comb generation. The major contribution of this thesis is the development of an improved dispersion measurement scheme which reduced the complexity of the previous design and simplified the measurement process. The modified dispersion measurement scheme, which uses the FSR evolution and spectroscopy method, can measure dispersion very precisely and in a more efficient way.

1. INTRODUCTION

On-chip microring resonator has been very popular recently because of their compact design, low power, high Quality factors, good control of Free Spectral Range (FSR) and many other uses in different areas. Apart from being used in spectral filters [1], microring resonator have very useful applications in cavity electrodynamics and laser cavities [2–4], molecular sensing [5], nonlinear optical effect based applications for example Second harmonic and Third harmonic generation [6, 7], parametric oscillation [8], four wave mixing [9, 10], Raman Lasing [11–14] etc. Microring resonators have also been used to implement Delay lines [15], Bio-sensing [16] etc. Characterization of these chips is important to get some important parameters like Quality factors, Free Spectral Range (FSR) or dispersion, which plays important role in their applications. Depending on those parameters they can be used to generate coherent frequency combs [17,18], soliton generation [19] and many other exciting applications.

In this thesis some of the optical characterization methods for On-Chip Silicon Nitride microring resonators are discussed. The materials that was used to fabricate the waveguides was Silicon Nitride and there are several reasons for using that. Firstly Silicon Nitride is a CMOS-compatible material and our goal is to make on-chip microring resonators. Also the dimension and repetition rate can be easily fabricated for Silicon Nitride waveguides. Large Band-gap for silicon Nitride is another reason because of which we get low nonlinear absorption and finally for larger Kerr non-linearity of Silicon Nitride, which is approximately a factor of ten greater than silica [20]. In this thesis all the chips that were characterized are Silicon Nitride chips unless otherwise mentioned.

The optical characterization basically means some of the measurement technique by which we can get basic and useful optical properties of a sample. Generally optical characterization includes both the time and frequency domain characterization. But in this thesis, we tried to focus on some of the major frequency domain characterizations which are: Transmission Spectrum measurement, Quality Factor Measurement, Dispersion measurement and Optical Frequency Comb generation. In this chapter, we are going to mention what a microring resonator is and briefly describe basic operation principle for microring resonator. We also mention the organization of the thesis at the end of this chapter. All the basic definitions related to the measurement processes are described in individual chapters later.

1.1 Microring Resonators

An optical microring resonator is a set of waveguides which consists of one or more input or output waveguides, through which the power is sent or received and one or more closed waveguides in which power is coupled and circulated. The input waveguide, through which we send the light in, is usually called the input bus waveguide as it guides the input light. The closed waveguide, in which power is coupled and circulated, can be of any shape, but the most common shape is a circular ring.

A microring resonator usually have two ports, an input port-through which the light is sent in and a through port by which light comes out as shown in Fig 1.1. When there is through port only, there is only one waveguide and the input light couples inside the microring via the coupling coefficient κ, circulates around the cavity. We only have one coupling region in this case. But occasionally we have another port, which is called drop port. When we have drop port in design that usually couples power from the field that develops inside the microring. So a separate waveguide takes power from the ring after the ring takes power from the input bus waveguide.

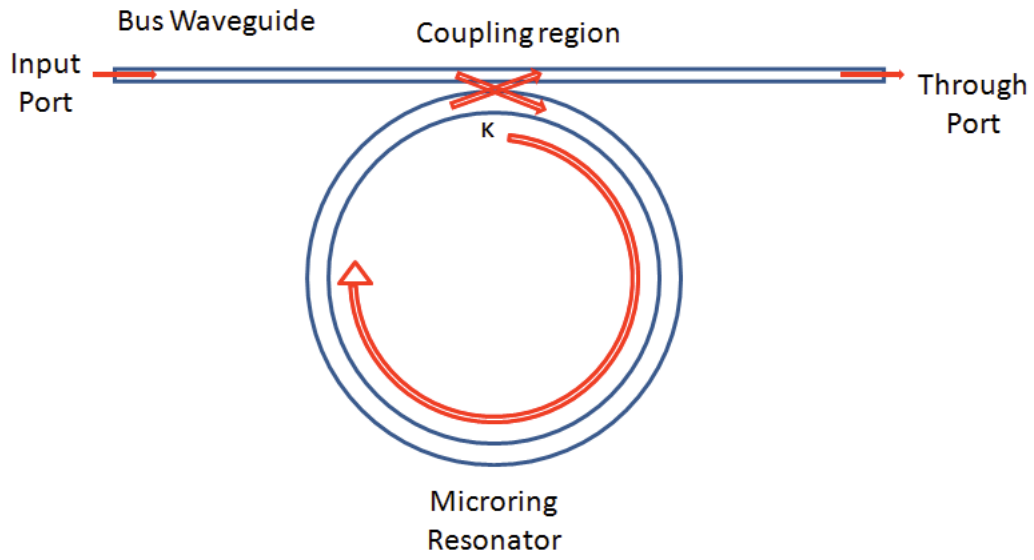

Fig. 1.1. A simple microring structure with through port only. There is only one bus waveguide and one coupling region.

In case of microring with drop ports, we have two bus waveguides, one is the same as mentioned before, with one input port and one through port as shown in Fig. 1.2. Another waveguide contains the drop port. In this case we have two coupling regions. The input light couples inside the microring via the coupling co-efficient κ_1 and the light is again coupled to the drop waveguide from the ring via another coupling co-efficient κ_2 and reaches the drop port. In this case, we get power from both the through and the drop port. It is notable that either either waveguide can be used as input waveguide. So the definition is not that strict for which one is through and which one is drop port. They are interchangeable depending on where we are putting the input light source.

When we send some light through the input waveguide of the microring resonator, some part of light is coupled to microring depending of the wavelength of the light and some of the design parameters of the microring, the rest of the light is transmitted to the output port via the input bus waveguide. The coupled light circulates inside

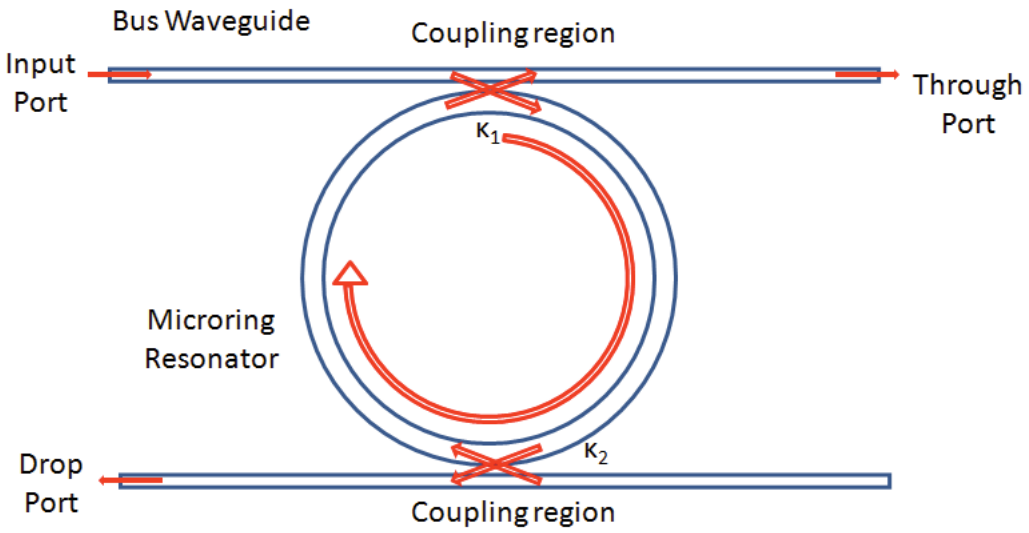

Fig. 1.2. A simple microring structure with both the through port and the drop port. We have two bus waveguides and two coupling regions.

the cavity by internal reflection and suffers some losses due to sidewall roughness, intrinsic absorption of waveguide material and scattering losses due to bending at the edges. On the other hand as the light completes one round trip, it interferes with the incoming light constructively and thus the light intensity inside the microring is build up.

The coupling of light critically depends on the gap between the ring and the input bus waveguide, the effective coupling length along which the coupling of light takes place and the refractive index of the medium between the two waveguides.

As mentioned above, microresonator has some characteristic internal losses due to the sidewall roughness, bending loss, waveguide losses and material absorption losses inside the microring. These losses are termed as intrinsic losses. Again, when we couple some light inside the microresonator, depending on the design parameters, some loss occurs during the coupling of light inside microresonator and that is termed

as coupling loss. Now, depending on two types of losses inside the microring, we can define the following coupling schemes for microring resonator:

1. When intrinsic loss> coupling loss, the scheme is called under-coupled. In this case the transmitted light to the through port is higher than the light coupled into the microring and the phase shift is less than 180 degrees. Under coupling can be achieved by increasing the gap size between the ring and the bus waveguide.

2. When intrinsic loss = coupling loss, the scheme is called critically-coupled. In this case no light is transmitted to the output as the light that comes out of the microring suffers 180 degree phase shift and it interferes with the light going to the though port destructively.

3. When intrinsic loss< coupling loss, the scheme is called over-coupled. In this case, the phase shift is more than 180 degrees and we can achieve this type of coupling by reducing the gap size between the ring and the bus waveguide.

1.2 Organization of This Thesis

In chapter 2, we will discuss about the Transmission Spectrum and Quality Factor measurement. We will describe the set up to measure transmission spectrum and the information that we can obtain from it. We will also focus on how we can measure Quality factors after measuring transmission spectrum.

Chapter 3 is the most important contribution in this this, where we will discuss the Dispersion measurement scheme. Starting from the first broadband spectroscopic method to obtain dispersion in microring, we will describe a modified dispersion measurement set up along with the algorithm and measurement technique.

In Chapter 4, we will briefly describe the principle of comb generation and the Comb generation set up that we use for generating optical frequency combs.

In chapter 5 we will try to show some of our measured results for one of our designed chips. We will also try to show some simulated results too and compare them with our experimental data.

And finally the summary of the thesis is in the conclusion chapter.

2. TRANSMISSION SPECTRUM AND QUALITY FACTOR MEASUREMENT

Transmission spectrum and Quality Factor are probably the two very basic and the most important optical characterizations for on-chip microresonator. A lot of optical characteristics depend on the quality factor the microring resonator. For example, optical frequency comb generation for microring requires certain quality factor and extinction ratio. In this chapter, we are going to describe the set up that we use for measuring transmission spectrum along with some important things that we can obtain from it. In section 2.1, we will briefly discuss what a transmission spectrum is along with some key features like Free Spectral Range (FSR) and Extinction Ratio (ER). In section 2.2, we will describe the basic transmission spectrum measurement scheme that we use for measuring transmission spectrum. In section 2.3, we define the Quality factor and discuss how we can extract quality factor from any resonance of transmission spectrum via curve fitting. In section 2.4, we mention the importance of transmission spectrum measurement and the things that we can obtain from it.

2.1 Transmission Spectrum

The transmission spectrum is obtained by plotting the transmittance for the system. Transmittance is defined as the ratio of the transmitted power to the input power. Let us consider a microring resonator without the drop port as shown in Fig 1.1. It has through port only and through the input port we send some light from a laser source and receive the output light from the through port. We want to see the transmission spectrum for this resonator, so we start with calculating transmittance. We can use the couple-mode theory described in [21] to calculate the transmittance.

Let us consider that the microring that we are considering can support a traveling wave of amplitude A(t). The ring can be considered as a weakly damped resonator with energy amplitude a(t), normalized in such a way that $|a(t)|^2$ gives the total energy in the ring. Now, the time rate change of energy inside the resonator can be described as [1]:

$$\frac{d}{dt}a = (j\omega_0 - \frac{1}{\tau})a - j\mu s_i \tag{2.1}$$

where, ω_0 is the resonant frequency of that resonator, s_i is the incident wave amplitude, μ is the mutual coupling between the ring and the bus waveguide, $\frac{1}{\tau}$ is the amplitude decay time constant for the oscillator $=\frac{1}{\tau_c} + \frac{1}{\tau_i}$, where $\frac{1}{\tau_c}$ is related with the coupling losses between the ring and the bus waveguide and $\frac{1}{\tau_i}$ is related with the intrinsic losses such as material absorption loss, scattering and bending losses etc. If the transmitted wave has an amplitude of s_t, then we can write [1]:

$$s_t = s_i - j\mu a \tag{2.2}$$

The decay rates can be calculated by providing some input power and then allow it to decay inside the cavity, In that case we can write the time variant energy inside the ring as [1]:

$$|a(t)|^2 = |a_0|^2 exp(-\frac{2t}{\tau_c}) \tag{2.3}$$

In this case, the intrinsic losses has been neglected or considered very small. Thus, the transmitted power can be written as [1]:

$$|s(t)|^2 = \kappa_c^2|A(t)|^2 = \kappa_c^2|a(t)|^2\frac{v_g}{2\pi R} \tag{2.4}$$

where, v_g is the group velocity and R is ring radius. mutual coupling μ and $\frac{1}{\tau_c}$ are related by energy conservation law. μ is related to κ_c by the following relation [1]:

$$\mu^2 = \kappa_c^2 \frac{v_g}{2\pi R} = \frac{2}{\tau_c} \tag{2.5}$$

Now, the solution of equation (2.1), considering a steady-state incident field s_i with frequency ω, can be written as [1]:

$$a = \frac{-j\sqrt{\frac{2}{\tau_c}}}{j(\omega - \omega_0) + \frac{1}{\tau}} s_i \tag{2.6}$$

Introducing this in equation (2.2), we get:

$$s_t = \frac{j(\omega - \omega_0) + \frac{1}{\tau} - \frac{2}{\tau_c}}{j(\omega - \omega_0) + \frac{1}{\tau}} s_i \tag{2.7}$$

Thus transmittance can be written as:

$$T = \frac{|s_t|^2}{|s_i|^2} = \frac{(\omega - \omega_0)^2 + (\frac{1}{\tau} - \frac{2}{\tau_c})^2}{(\omega - \omega_0)^2 + (\frac{1}{\tau})^2} \tag{2.8}$$

Now replacing τ by κ using equation (2.5) and using $|f - f_0| = \frac{c|\lambda - \lambda_0|}{\lambda^2}$, we can rewrite equation (2.8) as:

$$T = \frac{(\lambda - \lambda_0)^2 + (\frac{v_g \lambda^2}{8\pi^2 Rc})(\kappa_c^2 - \kappa_i^2)^2}{(\lambda - \lambda_0)^2 + (\frac{v_g \lambda^2}{8\pi^2 Rc})(\kappa_c^2 + \kappa_i^2)^2} \tag{2.9}$$

Where, κ_c^2= fraction of power losses due to coupling of power to the ring from bus waveguide, κ_i^2=fraction of intrinsic power losses. Thus at resonance (when $\lambda = \lambda_0$), the transmittance depends on κ_c and κ_i. Again, we see when we have κ_c=κ_i, we have T=0, which means critical coupling. thus we can redefine the definitions of different coupling schemes with the help of these coefficients:

1. Under-coupled: When $\kappa_c < \kappa_i$ or in other words, the ratio of $\frac{\kappa_c}{\kappa_i}$ <1.
2. Critically Coupled: When κ_c=κ_i or in other words, the ratio of $\frac{\kappa_c}{\kappa_i}$=1.
3. Over-coupled:When $\kappa_c > \kappa_i$ or in other words, the ratio of $\frac{\kappa_c}{\kappa_i}$ >1.

A sample transmission spectrum is shown in Fig. 2.1. As we can see from the figure, some of the important terms related to Transmission Spectrum are Free Spectral range (FSR), Extinction Ratio (ER) which are explained in next few subsections; and the Quality factor, which is explained in next section.

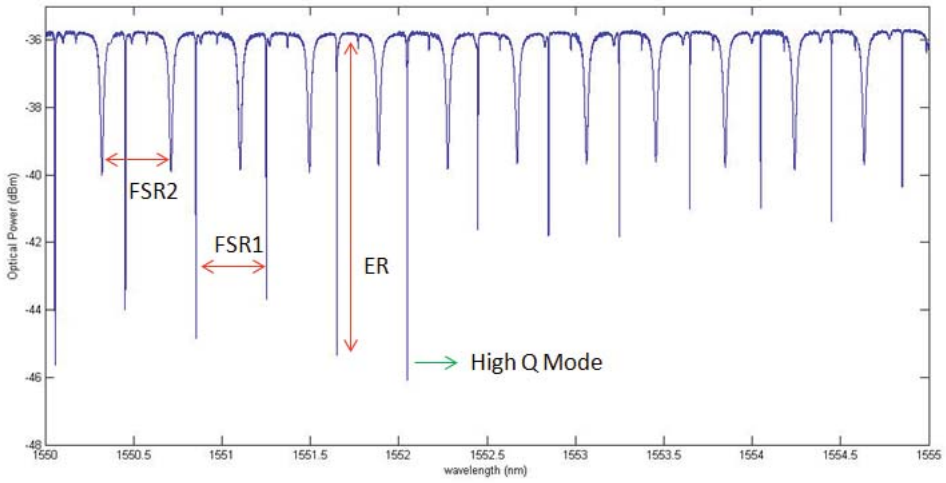

Fig. 2.1. A sample Transmission Spectrum for a Microring Resonator. Each dip corresponds to a resonance frequency that the microring resonator can support. FSR can be calculated from two consecutive resonant frequencies of the same mode family. FSR_1= FSR for mode family 1 and FSR_2=FSR for mode family 2. We can also estimate the number of modes that the microring can support. Here, the number of modes=2. Also high Q mode family is also shown in this figure.

2.1.1 Free Spectral Range (FSR)

Free Spectral Range (FSR) of an optical microresonator is defined as the spacing in frequency or wavelength between two maxima of the dropped power or minima of the through power. FSR can be obtained from transmission spectrum very easily. It is just the difference between two successive resonance frequencies or wavelengths for the same mode family. Usually FSRs for a particular mode should be the same over the wavelength of interest. But because we have dispersion, usually they do not remain the same. Also FSR for different mode families are different. If a microresonator can support multiple modes, then the fundamental mode usually have the highest FSR. Fig 2.1 shows a sample transmission spectrum and FSRs for two different mode families are termed as FSR_1 and FSR_2.

Mathematically, FSR can be defined (in frequency) as [22]:

$$FSR_f = \Delta f_{FSR} = \frac{c}{n_g L} \tag{2.10}$$

Where, c=velocity of light, n_g= Group index of the cavity material, L=Length of the cavity. FSR is also the inverse of round-trip time. If the round-trip time for the cavity is T_R, then:

$$T_R = \frac{1}{FSR_f} = \frac{n_g L}{c} \tag{2.11}$$

To express FSR in wavelengths, we can just convert it in wavelength from frequency difference by the well known formula:

$$f = \frac{c}{\lambda} \Rightarrow \Delta f_{FSR} = -\frac{c}{\lambda^2} \Delta \lambda_{FSR} \tag{2.12}$$

Thus, FSR can be calculated in wavelengths as:

$$FSR_\lambda \approx \frac{\lambda^2}{n_g L} \tag{2.13}$$

If the ring is circular then we can replace L by the rings circumference $2\pi R$. Thus equation (2.10) and (2.13) becomes:

$$FSR_f = \frac{c}{2\pi R n_g} \tag{2.14}$$

$$FSR_\lambda \approx \frac{\lambda^2}{2\pi R n_g} \tag{2.15}$$

where R= Radius of the microring.

2.1.2 Extinction Ratio (ER)

Extinction ratio (ER) is fundamentally defined as the ratio of two optical signals generated by an optical source. Mathematically, we can express it as-

$$ER = \frac{P_2}{P_1} \tag{2.16}$$

Where, P_2 is the received power and P_1 is the transmitted power. Usually it is expressed in dB unit, in which case we write it as:

$$ER = -10log\frac{P_2}{P_1}(dB) \tag{2.17}$$

In microresonator, we can define Extinction Ratio as the ratio between transmitted power and input power. Extinction Ratio can simply be obtained from the transmission spectrum. The difference between the maximum and minimum point in a particular resonance gives us the Extinction Ratio. For example if we see Fig 2.1, the Extinction Ratio for the marked resonance is around 10.5 dB.

Extinction Ratio plays a vital role in defining the coupling scheme of the microresonator. We have defined difference coupling types in chapter 1 and section 2.1. When the Extinction Ratio is highest, we get critical coupling. Extinction Ratio is also important because if Extinction Ratio is too small, then we cannot probably use that for comb generation. Thus Extinction Ratio plays a vital role in the application of microring resonator.

2.2 Transmission Spectrum Measurement Setup

The set up for transmission measurement is pretty simple. We have a tunable laser source which sends power to input bus waveguide and from there power is coupled to the ring. We also have a power sensor which senses the output power from output bus waveguide. The set up is shown in figure 2.2.

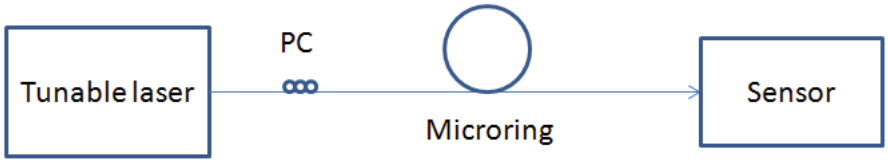

Fig. 2.2. A simple set up for measuring Transmission Spectrum of a microring resonator. PC= Polarization Controller. Tunable Laser= Agilent 81680A or Agilent 81940A or New Focus Laser, Sensor=HP81632A or 81634B

As shown in Fig. 2.2, the transmission measurement set up contains a tunable laser source. In our lab we have 3 different tunable laser sources that we can use as the laser source namely New Focus laser, Agilent 81680A and Agilent 81940A. there is a sensor mounted in each of the Agilent laser sources namely HP81632A for Agilent 81680A and 81634B for Agilent81940A. When we use New Focus laser, we can simply use some power meters or some power sensors for example ThorLabs PM100A power meters, ThorLabs PM20 power meters and ThorLabs S145c sensor. ThorLabs PM20 power meters can measure power from -60 dBm to +13dBm, but ThorLabs S145c sensor can sense up to 3W of power.

The light is coupled into the microring resonator using a 5 axis translational stage and tapered lens fiber. The polarization controller is used to match the polarization for maximum output.

2.3 Quality Factor

Quality Factor is a very important parameter for microring resonator. Quality Factor or popularly known as Q factor measures the frequency selectivity or sharpness of the resonance. It is a measure of the strength of the damping of its oscillations or for relative line-width. Q-factors are related to the stored energy in the microring resonators. The higher the quality factors are, the lower the losses are. Thus it plays a vital role in application of microring resonators.

Q-factor can be defined in two different ways, which are not equivalent, but as Q gets higher, they get very very close to each other:

The most common definition is probably by using bandwidth as the resonance. For this definition Q of a microring resonator can be defined as [23]:

$$Q = \frac{f_r}{\Delta f} = \frac{f_r}{FWHM} \tag{2.18}$$

where, f_r is the resonant frequency of the microring resonator and FWHM= Full Width at Half Maximum. Thus from equation (2.18) we see Q is higher for lower Δf. So when Δf is very small, Q is very high.

Experimentally we use this definition to calculate the estimated value of Quality factors from transmission spectrum data. Another definition can be given from energy storage perspective. Q can be defined as the time averaged stored energy to the energy dissipated per cycle [24]:

$$Q = 2\pi \frac{E_{stored}}{E_{dissipated}} = \omega\tau \tag{2.19}$$

where, E_{stored} is the energy stored by microring per optical cycle, $E_{dissipated}$ is the energy dissipated by the microring per optical cycle, ω=Resonant frequency and τ=$\frac{1}{\kappa}$= cavity lifetime, κ= cavity decay rate=κ_i+κ_c, κ_c=coupling loss rate and κ_c=Coupling loss rate.

From the second definition, we see that we need to excite the microring to a certain level and then allow the power inside the microring to decay. From the rate of power decay we can get Q-factor. From this definition, the Q factor of a microring is related to the round trip losses, coupling losses, bending and scattering losses in the microring. The lower the losses are, the higher the Q. Alternatively, if a device has higher Q, it can store more energy. Thus, when a microring has drop port, it's quality factors will be lower than a microring without drop port or through port only.

The Quality factors for a microring resonator can be expresses in two different ways which are pretty common in literature: One is Loaded Q factor (Q_L) and another is Intrinsic Q factor (Q_i). The fundamental difference between them is that we get intrinsic Q without considering coupling loss, that mean we only consider all the losses inside the microring without coupling it to the bus waveguide. That means we only consider material absorption loss, surface roughness loss, bending and scattering loss and radiation loss inside the microring. But when we couple the microring to the bus waveguide, then we get overall Q or loaded Q. From this definition, it is pretty obvious that for any microring resonator, loaded Quality factor will always be less than Intrinsic Quality factor.

Now, the Quality factors can be calculated from transmission data by using the method described in [25]. If κ_c^2 is the fraction of power that couples into microring from bus waveguide and κ_i^2 is the fraction of intrinsic power losses as mentioned above (material absorption loss, bending loss, scattering due to surface roughness etc) per round trip, then following the same method we describe in section 2.1, the transmittance for the through port can be estimated as [25]:

$$T_{through} = \frac{(\lambda - \lambda_0)^2 + (\frac{FSR}{4\pi})^2(\kappa_c^2 - \kappa_i^2)}{(\lambda - \lambda_0)^2 + (\frac{FSR}{4\pi})^2(\kappa_c^2 + \kappa_i^2)} \tag{2.20}$$

Now from experimental transmission spectrum measurement we can use curve fitting method to match the transmission with the transmittance described in equation (2.20) and from there we can estimate the value of Q for that reference. By using the same method, we can measure Q for all the resonances from transmission spectrum.

2.4 Importance of Transmission Measurement and Q factors

As mentioned before, Transmission Spectrum is simple but one of the most important characterization processes for on-chip microresonator. If there is no microring

resonator in our setup, the transmission spectrum would possibly be a flat line without any resonances, which corresponds to the laser power from the Diode Laser source. But when we have a microring resonator, due to the power coupling and losses inside the microcavity, we get different resonances corresponding to the cavity modes of the microring. Each mode of the cavity gives rise to a family of resonances and depending on different design parameters we can estimate how many modes can exist in certain type of microcavity.

There are a lot of information that we can obtain from transmission spectrum. The most important thing that we can obtain from transmission spectrum is the Free Spectral Range (FSR). As mentioned in section 2.1 and Fig 2.1, the FSR can be calculated from any two consecutive resonant frequencies of the same mode family. A very important fact is that, FSR actually depends on the dispersion of the chip. If there is no dispersion all the FSRs will be the same and there will be no change wherever we calculate the FSR. But in presence of dispersion, FSRs will change and later in chapter 3, we have shown how we can calculate dispersion from such kind of FSR evolution.

Another important thing that we can identify and measure the high Q mode from transmission spectrum. In fig 2.1, we have marked the high Q mode as it is pretty obvious from the definition of Q factors, which is discussed in section 2.3. As mentioned in previous subsection, if a device has higher Q, it can store more energy. This is very important in case of comb generation, when we need certain threshold power to generate the comb lines. This is a big concern for us as the fiber amplifier that we have, they cannot amplify beyond certain limit. But if the Q is high, as we will see in chapter 4, the threshold for comb generation is reduced. And we can generate comb with the fiber amplifiers that we have. Thus, Quality factor plays a critical role in comb generation.

We can also estimate how many modes can sustain inside the microcavity for a specific polarization. The number of modes will be equal to the number of mode families in the transmission spectrum. This is an easy process when the number of the mode families is less and their Extinction Ratio is pretty different. When we have mode families of same extinction ratio, sometimes it becomes difficult to separate the modes. As shown in figure 2.2, we can see that this microring can contain 2 mode families for the given range of wavelength.

Another important thing that we can observe from transmission spectrum is that we can see if there is any mode interaction occurring between the modes or not. Mode crossing plays a vital role in the generation of optical frequency comb in normal dispersion regime as described in [17]. Again, an important feature of transmission spectrum is that we can see the Extinction Ratio of the resonances, which is crucial in coupling scheme of the micro-resonators. The Extinction Ratio is highest when we are very close to critical coupling. Also from experimental experiences, we cannot generate comb for very low extinction ratios. Thus we can choose a suitable resonance for comb generation from transmission spectrum. We have tried to briefly discuss optical frequency comb generation in chapter 4.

3. DISPERSION MEASUREMENT

In this chapter, we will introduce the dispersion measurement scheme. The major contribution in this thesis is the modification of the previous dispersion measurement set up. We will start with the definition of dispersion in section 3.1. Then we will try to describe previous dispersion measurement set ups along with the modified set up in section 3.2. In section 3.3 we will try to show some mathematical formulation of how we can measure dispersion from FSR evolution. Finally we will describe our dispersion measurement set up and describe the measurement procedure along with discussing what kind of improvement the modified dispersion measurement can give to us in section 3.4.

3.1 Dispersion

Dispersion is a very important parameter for microring resonator. The word dispersion generally means the action or process of distributing things over a wide area. In Optics the term dispersion results in similar type of thing- spreading of the pulse. Dispersion generally occurs when different frequency components travels at different speed. Or in other words, when the group velocity depends on frequency. The result of such thing is that different frequency component has different round trip in the cavity, resulting in the pulse broadening. When the pulse is broadened it actually can cause a lot of unwanted situations including distortion of data, reduction of bandwidth etc. In case of comb generation, dispersion is crucial as it limits the maximum achievable comb bandwidth [26].

When light passes through any dispersive media, the system adds a spectral phase to that light. If the length of the medium is L and the spectral phase introduced by the medium is $\psi(\omega)$, then we can write [27]:

$$\psi(\omega) = -\beta(\omega)L \tag{3.1}$$

Mathematically dispersion refers to the frequency dependence of propagation constant β of light in the medium. From the definition of propagation constant β, we can write:

$$\beta(\omega) = \frac{2\pi}{\lambda_0} n(\omega) = \frac{\omega}{c} n(\omega) \tag{3.2}$$

where, λ_0 is the wavelength of light in vacuum, c is the velocity of light in vacuum and n(ω) is the frequency dependent refractive index of the medium.
Now, the propagation constant $\beta(\omega)$ can be written in Taylor's series as [27]:

$$\beta(\omega) = \beta(\omega_0) + \frac{\partial\beta}{\partial\omega}(\omega - \omega_0) + \frac{1}{2}\frac{\partial^2\beta}{\partial\omega^2}(\omega - \omega_0)^2 + Higher\ Order\ Terms \tag{3.3}$$

Ignoring small effects from higher order terms of equation (3.3), we can rewrite it as:

$$\beta(\omega) = \beta_0 + \beta_1(\omega - \omega_0) + \beta_2(\omega - \omega_0)^2 \tag{3.4}$$

where, β_0 is the zeroth order dispersion and it corresponds to a constant phase shift in the form of equation (3.1). β_1 is the first order dispersion, which is the inverse of group velocity v_g and it can be expressed as [27]:

$$\beta_1 = \frac{\partial\beta}{\partial\omega}|_{\omega=\omega_0} = \frac{1}{v_g} \tag{3.5}$$

This introduces a constant group delay [27]:

$$\tau = -\frac{\partial \psi}{\partial \omega} = \beta_1 L = \frac{L}{v_g} \tag{3.6}$$

It is worth noting that this constant delay does not affect the shape of the pulse. The third term in equation (3.4) is β_2 which refers to second order dispersion and that is the most common parameter to describe dispersion in microring resonators. The term $\beta_2 = \frac{\partial^2 \beta}{\partial \omega^2}$ is also called Group Velocity Dispersion (GVD). Again, Group Velocity Dispersion (GVD) is related to the Group Delay Dispersion (GDD) by the fact that GVD is GDD per unit length [24], which is pretty obvious from equation (3.1) and equation (3.6):

$$GVD = \beta_2 = \frac{GDD}{L} \tag{3.7}$$

In fiber optics, dispersion is usually described in terms of dispersion co-efficient (D) which can be expressed as [27]:

$$D = \frac{\partial \beta_1}{\partial \lambda} = -\frac{2\pi c \beta_2}{\lambda^2} \tag{3.8}$$

The unit of D is ps/nm-km and it actually gives the group delay difference of two optical pulses after propagating certain distance in the optical fiber at certain wavelength. Depending on the sign of D we define two distinct type of dispersion:

1) When D>0, the dispersion is called Anomalous Dispersion.
2) When D<0, the dispersion is called Normal Dispersion.

It is worth noting that we get the frequency dependent refractive index for material dispersion from the famous Sellmeier equation [28]:

$$n^2(\lambda) = 1 + \sum_i \frac{B_i \lambda^2}{\lambda^2 - C_i^2} \tag{3.9}$$

where B_i and C_i are Sellmeier coefficients and their values can be found from [29].

3.2 Broadband Precision Spectroscopy to Measure Dispersion

3.2.1 Basic Dispersion Measurement Setup

The spectroscopic method to measure the dispersion by using a frequency comb was first introduced in [30]. The experimental set up is shown in Fig 3.1. The fundamental concept for this method was to accurately locate the resonances from transmission spectrum by generating RF beat notes using an external diode laser (New Focus laser) and an erbium fiber laser based frequency comb (Menlo System GmbH). The beat notes are used like a frequency ruler which are detected by a fast photo-diode. To increase the number of beat notes for better resolution two Band Pass Filters of 30 MHz and 75 MHz were used which in turn give rise to four frequency marker within each interval of one repetition rate of Menlo Comb (250 MHz).

A frequency marker was recorded when a beat note falls within the pass band of the Band Pass Filter (1 MHz) or when the diode laser frequency was equal to [30]:

$$f_D = f_{ceo} + n f_{rep} \pm f_{BP} \tag{3.10}$$

where, f_D=Diode laser frequency, f_{ceo}= Carrier envelope offset frequency of Menlo Comb, f_{rep}= Repetition rate of Menlo comb and f_{BP}= Center frequency of Band Pass Filter.

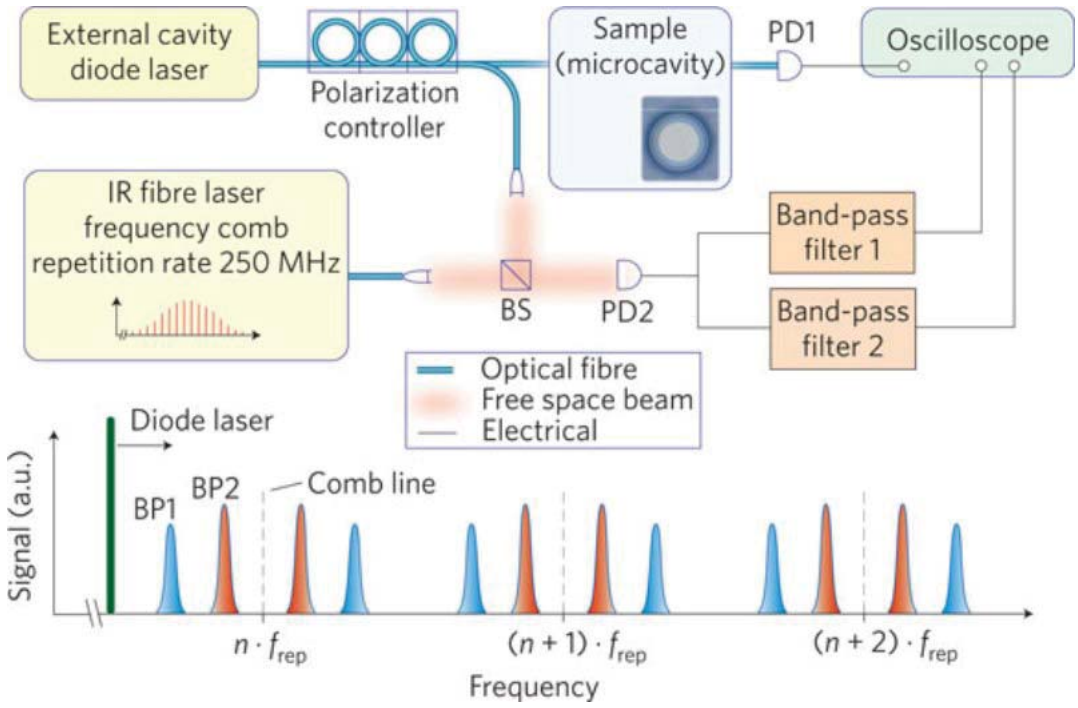

Fig. 3.1. Dispersion measurement Scheme depicted in [30]: New Focus laser beats with an Menlo comb and generate four beat notes in each repetition period of Menlo comb. This Figure is taken from [30]

The calibration peaks were recorded using a four channel oscilloscope which can support 10 million data points per channel. That leads to a resolution of 370 kHz per data point for 30 nm scan range and each measurement gave rise to more than 64000 calibration peaks. An illustration of frequency markers is shown in Fig. 3.2.

After getting calibration peaks and transmission spectrum we could precisely calculate the resonance frequencies of the microcavities because all the resonances will fall on or within any two frequency markers as shown in Fig 3.2. Now by knowing the difference between consecutive resonance frequencies we can find the Free Spectral Range (FSR) of any particular mode. Then by plotting FSRs and taking the slope and intersection after linear fitting, we can calculate the dispersion for the microcavity. The detail mathematical formulation of the process is shown in section 3.3.

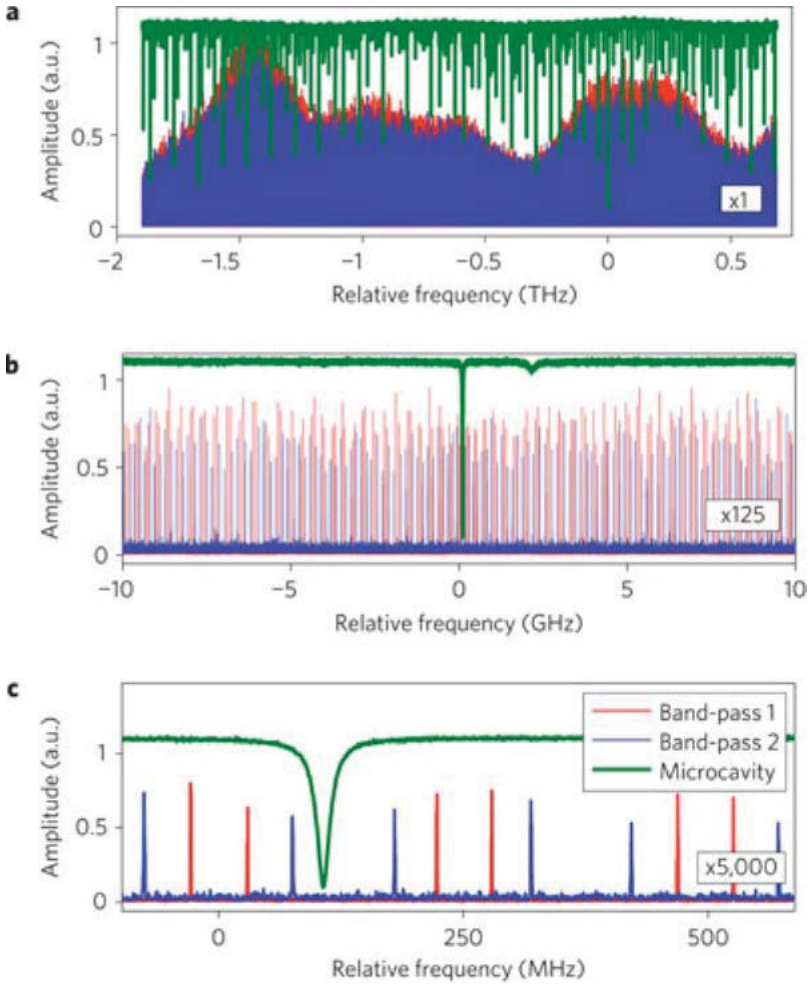

Fig. 3.2. Transmission spectrum at different frequency spans: a) 2.5 THz b) 20 GHz and c) 500 MHz. Figure c) shows four calibration markers that generated within each interval of the repetition rate of Menlo comb. This Figure is taken from [30]

3.2.2 Initial Dispersion Measurement Setup

The dispersion measurement set up described in section 3.2.1 was a very important contribution in dispersion measurement of microcavity since this process could measure dispersion very precisely. But a drawback of that set up was that the frequency marker could only give the relative positions of the frequencies, not the absolute ones or in other words, not the real frequencies. That issue was addressed by one of our

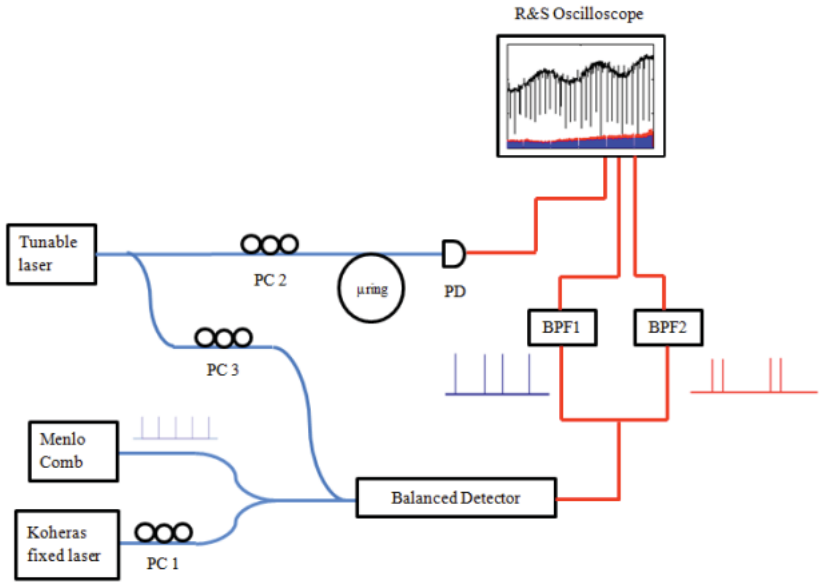

Fig. 3.3. Modified Dispersion measurement set up described in [31] including the Koheras fixed laser to find absolute positions of frequency markers. This figure is taken from [31]

previous group member Steven Chen in his thesis [31]. The modified set up suggested in [31] is shown in Fig 3.3.

In this set up, the absolute frequency issue was addressed by introducing a fixed laser with known wavelength (or frequency). This fixed laser couples with the New Focus laser through a 50-50 fiber optic coupler and then beats with the menlo Comb. Now, due to the beating of fixed laser and menlo comb, we get four extra frequency markers, which can be used as frequency references. The basic idea behind this was that as we know the frequency of the fixed laser, once we know the position of those markers, we can easily calculate the position of all the markers. The laser which was used as a fixed laser is Koheras laser and the wavelength of Koheras is 1541.76206 nm with an uncertainty of 0.000038 nm as shown in Fig 3.4 [31].

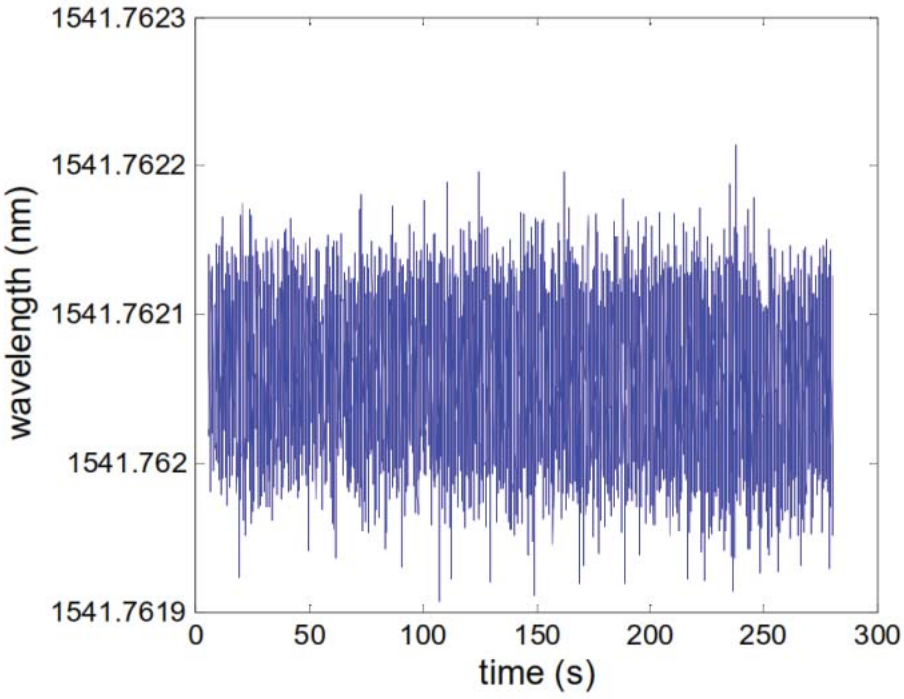

Fig. 3.4. The wavelength variation of fixed Koheras laser with time. This Figure is taken from [31]

3.3 Mathematical Formulation to Measure Dispersion from FSR Evolution

In this section we will show how we can measure dispersion from FSR evolution. This derivation is very much similar to the one derived in [31], except the fact that we have made some important corrections here. We will start with the definition of FSR. We can find FSR by measuring the transmission spectrum for the microresonator. As mentioned in chapter 2, we can obtain the resonant frequencies for all the cavity modes from transmission spectrum. The difference between two resonant frequencies for a particular mode gives us the Free Spectral Range or FSR for that particular mode.

We will start from equation (3.1) which gives us the relation between the spectral phase that arises due to dispersion and the propagation constant. Using that relation, we can write:

$$\psi(\omega) - \psi(\omega_0) = -[\beta(\omega) - \beta(\omega_0)]L \tag{3.11}$$

Now Ignoring higher order terms of equation (3.3), we can write:

$$\beta(\omega) - \beta(\omega_0) = \beta_1(\omega - \omega_0) + \frac{\beta_2}{2}(\omega - \omega_0)^2 \tag{3.12}$$

where $\beta_1 = \frac{\partial\beta}{\partial\omega} = \frac{1}{v_g} =$ inverse of group velocity and $\beta_2 = \frac{\partial^2\beta}{\partial\omega^2} =$ Second order dispersion as mentioned in section 3.1. Now from equation (3.11) we can write:

$$\psi(\omega) - \psi(\omega_0) = -[\beta_1(\omega - \omega_0) + \frac{\beta_2}{2}(\omega - \omega_0)^2]L \tag{3.13}$$

Now we can differentiate equation (3.13) with respect to ω and rewrite equation (3.13) as:

$$\frac{\Delta\psi}{\Delta\omega} = -[\beta_1 + \beta_2(\omega - \omega_0)]L \tag{3.14}$$

Now we can relate this with FSR by the fact that FSR is the difference in frequency for two consecutive resonances. The phase shift per FSR or phase shift between two consecutive resonances is 2π and we can write:

$$\Delta\omega = 2\pi\Delta f = 2\pi FSR \tag{3.15}$$

Thus,

$$\frac{\Delta\psi}{\Delta\omega} = \frac{2\pi}{2\pi FSR} = \frac{1}{FSR} \tag{3.16}$$

Therefore, from equation (3.14) we can write:

$$\frac{1}{FSR} = -[\beta_1 + \beta_2(\omega - \omega_0)]L \tag{3.17}$$

So,

$$FSR = -\frac{1}{L}\frac{1}{\beta_1 + \beta_2(\omega - \omega_0)} \tag{3.18}$$

Expanding the right side of equation (3.18) and ignoring higher order terms, we can write:

$$FSR = -\frac{1}{\beta_1 L} + \frac{\beta_2(\omega - \omega_0)}{\beta_1^2 L} \tag{3.19}$$

Now if we plot FSR vs Frequency, then it will give us a straight line $y = a_1 x + a_0$ with a slope $a_1 = \frac{\beta_2}{\beta_1^2 L}$ and a vertical axis intercept $a_0 = -\frac{1}{\beta_1 L}$. Thus the second order dispersion β_2 can be written as:

$$\beta_2 = -\frac{a_1}{a_0^2 L} \tag{3.20}$$

Thus, from equation (3.8), the dispersion co-efficient can be calculated as:

$$D = \frac{2\pi c a_1}{\lambda^2 a_0^2 L} \tag{3.21}$$

Now by doing linear curve fitting for FSR data points for different wavelengths or frequencies, we can find the values of a_0 and a_1. If we know the radius of the ring or the length of the microring, we know L. The velocity of light c is constant and the λ is the wavelength in which we want to measure dispersion. Therefore, we know all the parameters of equation (3.21), from which we can measure the dispersion co-efficient for the microring cavity.

3.4 Modified Dispersion Measurement Setup

It is true that introducing Koheras laser as a fixed wavelength laser solved the absolute frequency issue, but it caused another complexity in the measurement. From the set up shown in Fig 3.3, we can see that Koheras laser couples with New Focus laser through a 50-50 coupler and then they beat with the Menlo comb together to produce beat notes. In most of the cases, the beat notes produced from the beating of Menlo comb and New Focus laser does not coincide with the beat notes produced from the beating of Koheras laser and the Menlo comb. But when they coincide or overlap each other, it becomes very difficult to distinguish them and some of the markers may not be identified accurately as shown in Fig 3.5.

Again, if they overlap with each other, it becomes difficult to get the exact position of both the koheras and the frequency markers which can result in error in our measurement.

One way to solve this issue is to manually select the markers produced by Koheras and New Focus and create beat note manually exactly in the same position. But that is not an efficient way of doing it. Also if they are partially overlapped, this can cause additional errors.

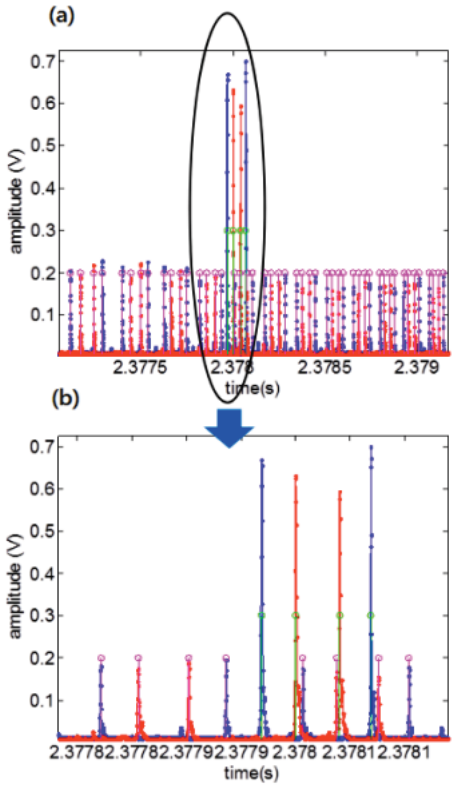

Fig. 3.5. Problem that arises from the overlapping of beating notes from Koheras and New Focus with the beating notes from Menlo and Koheras. Fig (b) is the zoomed version of Fig (a). This figure is taken from [31]

So in this thesis, we are introducing another set up, which is a modified version of the set up shown in Fig. 3.3. The modified Dispersion measurement set up is shown in Fig 3.6.

In this set up we have separated the fixed laser (Koheras) from Menlo comb and we beat it separately with New Focus in a separate channel (Channel 4) of the oscilloscope. And thus we avoided that complexity, but for this we had to add few more components to the setup.

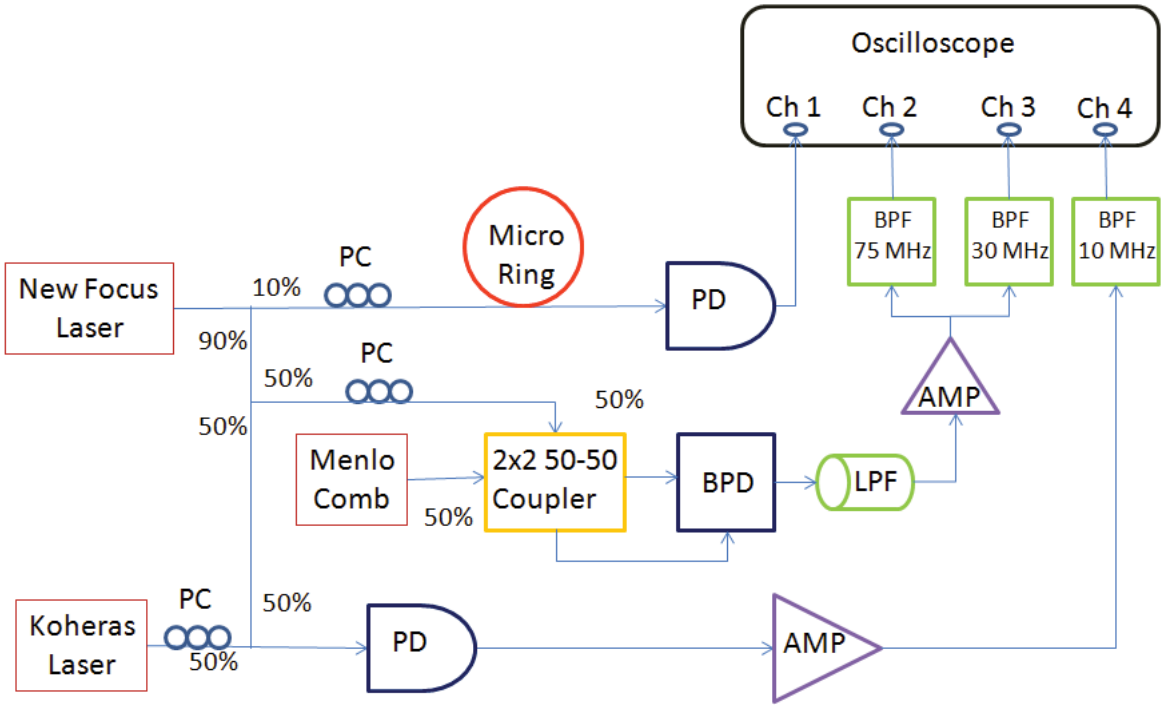

Fig. 3.6. Final dispersion measurement set up. The fixed laser (Koheras) is separated from Menlo comb and it beats with New Focus in a separate channel (channel 4) of the oscilloscope. PC: Polarization Controller, PD=Photo Diode, BPD= Balanced Photo Diode, LPF= Low Pass Filter, BPF= Band Pass Filter. For simplicity, attenuators and power supplies for amplifiers and balanced photo-diode are not shown in the figure.

3.4.1 Equipment used in Modified Dispersion Measurement Setup

There are few components that are common to all the setups and they serve the same purpose. For the convenience of a better understanding, we will briefly describe the functions of different components used in our setup mentioning major differences.

As the tunable laser source, we have used New Focus laser, same as before, shown in Fig. 3.7.

Fig. 3.7. New Focus tunable laser source that is used in our measurements. The picture is taken from [32]

But in this setup, the power that goes out of the New Focus laser is distributed little differently than the other setups. As we need to beat New Focus and Koheras separately, we have used a 90-10 coupler to split the output power of New Focus. Since, we need very small power for linear measurements, 10% power is sent to the stage via a polarization controller and an attenuator where the microresonator chip is coupled and the rest is used for beating purpose. Then the 90% power is split by a 1x2 50-50 coupler and one part of it goes through a polarization controller and at-

tenuator before beating with Menlo comb. Another part directly beats with Koheras laser via a 2x1 50-50 coupler.

As fiber laser frequency comb, Menlo system is used, same as before. Menlo comb gives us flat combs with a repetition rate of around 250 MHz. It couples and beats with a part of New Focus laser through a 2x2 50-50 coupler, goes through a Balanced Photo-diode, which suppresses common mode noises, Low pass Filter which removes all high frequency components, An Electrical Splitter which splits the signal equally into two separate branches and an Amplifier, which boosts the signal for better detection. Finally it goes to Channel 2 and 3 of the oscilloscope after passing through 75 MHz and 30 MHz Band Pass Filters respectively.

Koheras is used as fixed wavelength laser same as before, but in this time Koheras beats with a part of New Focus laser using a 2x1 50-50 coupler after passing through a Polarization controller. It is then converted to electrical signal via a photo-diode, boosted up little bit via an electrical amplifier and finally passed to the channel 4 of the oscilloscope using a 10 MHz Band Pass Filter.

Fig. 3.8. Rohde and Schwarz Oscilloscope, which is used to acquire data from our setup. The picture is taken from [33]

There are 3 +15V power supplies in this setup. Two of them gives bias voltages for electrical amplifiers and the other one gives power to the balanced photo-diode. The output of the chip microresonator is sent to the channel 1 of the oscilloscope using a photo-diode and via a load resistor of 110kΩ was used to properly detect the rise and fall of the resonances. We have used Rohde and Schwarz Digital Oscilloscope for our measurements as shown in figure 3.8.

3.4.2 Algorithm for obtaining dispersion from the frequency markers

The algorithm for obtaining dispersion from the acquired data is described in [31]. So that is not described here again in details as we followed the same algorithm. But we just want to mention the fundamental idea of the algorithm here very shortly. The first important thing is to set a threshold for all the frequency markers. Any peak above the threshold will be counted and below the threshold will be neglected. This is important because we get some small peaks due to the noise in the system and that may lead us to erroneous results if we consider those peaks. So we select a suitable threshold so that all the peak due to the noise doesn't come into consideration and at the same time, we get all the required frequency markers for our measurement.

In our code, we choose threshold in an adaptive manner. That means, we measure the maximum height of the markers and set a percentage (for example 30% or 20%) of it as the threshold value. But again we have to be careful because if some of our marker's amplitude goes beyond that threshold, we may miss a marker and that may cause error in our results. So, we need to check if we have found all the frequency markers properly or not. Also we can find out where we have the error and correct it accordingly by reducing the threshold a little bit or by manually adding a marker there or by properly optimizing the polarization and taking data again.

The next step is the find the exact position of the reference markers. We actually get two frequency markers from channel 4, which gives us information about Koheras laser's frequency. As we previously know the frequency of the Koheras laser, we basically can know the exact frequency of those frequency markers. If the frequency of the Koheras laser is f_k Hz, then those two marker positions would be f_k-10 MHz and f_k+10 MHz. To find the marker peaks, we follow the same procedure to find the peaks by using a threshold value. Once we detect the position of those markers, using simple algebra, we can find the exact frequency of those markers. And once we get the exact frequency of those reference markers, we can simply find the exact or real frequencies of all the frequency markers by simple interpolation method.

After we get all of our frequency markers properly, then we check the transmission data and find where the resonance falls into and find the real frequency of that point using simple interpolation. And then we manually assign the resonance numbers to each mode families and separately we can measure FSR for each family. After that, we can plot the FSR and by linear fit and using equation (3.21), we can calculate dispersion for that particular mode family.

4. OPTICAL FREQUENCY COMB GENERATION

In this chapter we will try to discuss the process of Optical Frequency Comb Generation from microring resonator. In section 4.1, we will try to go through some of the fundamental concepts about the frequency comb generation. In section 4,2, we will try to describe our frequency comb generation set up.

4.1 Optical Frequency Comb

Optical Frequency Combs are evenly spaced periodic spectral lines, which are discrete and the spacing between individual comb lines are constant along the whole spectrum. Thus an optical frequency comb can be used as an optical ruler as because if we know the comb frequency we can find any unknown frequency by beating that with the optical frequency comb. Optical frequency combs have been useful in many application where we need high repetition rate and high comb power [34] such as comb spectroscopy [30] or molecular fingerprinting [35], astronomical calibration [36] or arbitrary waveform generation [37] etc. A very related example of this is our dispersion measurement set up as described in section 3.1-3.4 where we have seen that a tunable laser beats with a frequency comb (Menlo Comb) to find the dispersion where the beat notes were used as ruler.

Optical frequency combs can be generated in many ways, but the most common method is using a mode-locked laser with stable frequency and repetition rate [24]. Fig 4.1 shows an example of mode locked frequency comb [27]:

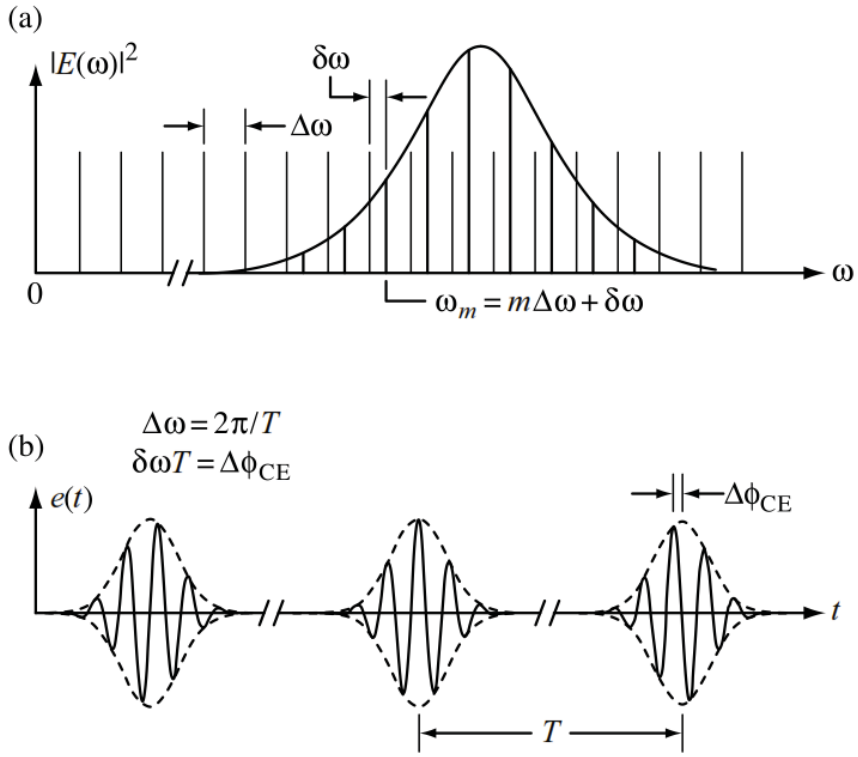

Fig. 4.1. Mode-locked frequency comb a) The offset frequency $\delta\omega$ is shown b) Pulse to pulse phase shift $\Delta\phi_{CE}$ is shown. The picture is taken from [27]

In general, the frequencies of individual comb lines for a frequency comb can be expressed as [27]:

$$f_m = mf_{rep} + f_{CEO} \tag{4.1}$$

where, f_{rep}=$\frac{1}{T}$ is the repetition rate of the laser, T is the period of the optical pulse as shown in Fig. 4.1 (b) and f_{CEO} is the carrier envelope offset frequency=$\frac{\delta\omega}{2\pi}$. It is difficult to obtain the value of carrier envelope offset frequency, which makes it quite difficult to obtain exact frequencies of the individual comb lines. However, the FSR in microring resonator can be controlled very easily. Also microring resonator allow us to reduce the size and can be implemented in chip level. So, for obtaining high repetition rate microring resonators have become very popular recently.

For microring resonators, optical frequency combs are generated by the interaction between a CW laser source with the modes of a high Q microresonator via Kerr nonlinearity [18]. The optical frequency comb in microring resonators are generated by a parametric frequency conversion which is based on the Four Wave Mixing (FWM) process. The parametric conversion must follow both the energy and the momentum conservation law. In this process two pump photons (ω_p) are absorbed at sufficient power and two side bands are generated as [34]:

$$2\omega_p = \omega_s + \omega_i \tag{4.2}$$

where $\omega_s = \omega_p + \Delta\omega$ and $\omega_i = \omega_p - \Delta\omega$ are generated side bands which must be equidistant to maintain energy and momentum conservation law. Now this process continues and the whole frequency comb is formed.If two pump photons generate side bands, they are usually called degenerate FWM. When one photon from pump interacts with one photon from nearby side bands and create two new side bands, then it is called non-degenerate FWM. An example of frequency comb generated from microring resonator is shown in Fig 4.2.

From literature, we can see that optical frequency combs were generated in both normal dispersion regime [17] and in anomalous dispersion regime [38,39]. It is worth mentioning that the process of comb generation is different in normal dispersion regime and in anomalous dispersion regime. In anomalous dispersion regime, the comb is generated with the aid of Modulation Instability (MI) gain and in normal dispersion regime, comb is generated close to mode crossing regime with the help of mode interaction [17].

In Microring resonator, the noise performance of generated frequency comb is very important. The noise in Kerr frequency comb is explained in details in [40]. Depending on the presence of noise and FSR spacing optical frequency combs can be classified in two types [37, 41]:

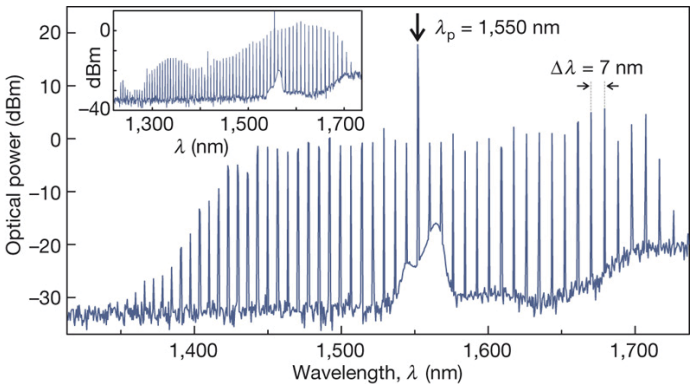

(a) A broadband Optical Frequency comb

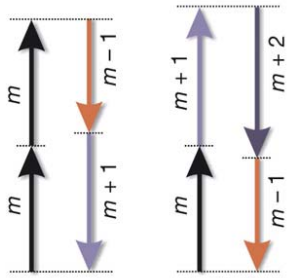

(b) Degenerate & non-degenerate FWM

Fig. 4.2. An example of Optical Frequency comb generated from microresonator via the parametric frequency conversion process. Fig a) shows the broadband frequency comb and Fig. b) shows the difference between degenerate and non-degenerate FWM process. The figure is taken from [18]

Type I comb: Optical frequency combs where the initially generated frequency comb lines are separated by single FSR.

Type II comb: Optical frequency combs where the initially generated frequency comb lines are spaced by multiple FSR. And then additional lines fill the gap in between to make the spacing between comb lines single FSR.

When the frequency comb lines are spaced by single FSR (Type I) comb, we can compress them to bandwidth limited pulse by using a pulse shaper [41]. Thus we can obtain coherence for type I comb which means that each comb line can have same spectral phase. The process of spectral line by line pulse shaping is shown in [37]. In contrast, type II combs, in which comb lines are multiple FSRs away, doesn't show such way of compression and show poor coherence [41, 42]. The reason is that when additional lines starts to fill the comb spacing, they may overlap in some region and generate intensity noise. An example of type I and type II comb is shown in Fig. 4.3.

A very critical issue about comb generation is that we need certain amount of threshold power to which can initiate the Four wave mixing process. If our input power to the chip is less than that, then we don't get any comb. The threshold power for comb generation depends on a few parameters among them Quality Factor is very important. The threshold power for comb generation can be expressed as [43]:

$$P_{th-comb} = \frac{\pi^2 R n_g^2 A_{eff}}{2\lambda_0 n_2} Q_{ext}\left(\frac{1}{Qext} + \frac{1}{Qin}\right)^3 \tag{4.3}$$

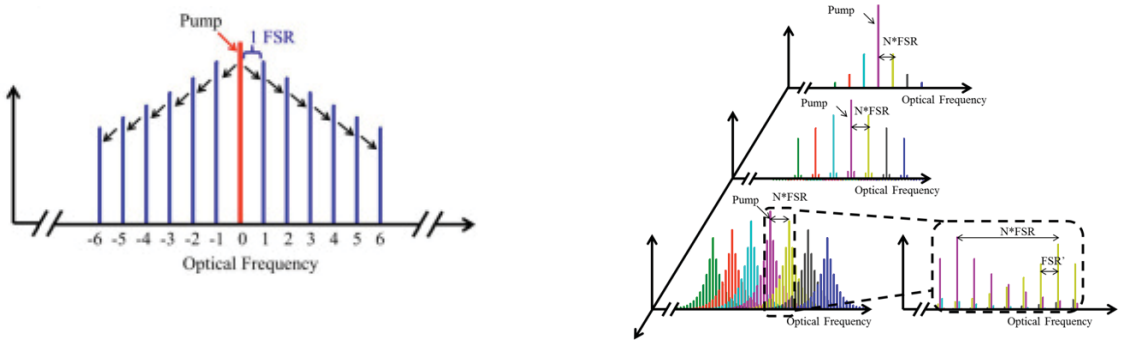

(a) Type I comb

(b) Type II comb

Fig. 4.3. An example of type I and type II comb. In type I comb, the frequency comb lines are single FSR away as shown in (a). In type II comb, they are initially multiple FSR away and finally they become single FSR after filling the spacing in between, as shown in (b). (a) is taken from [41] and (b) is taken from [40]

where, R= Average ring radius, n_g is the effective group index, A_{eff} is the effective area, n_2 is Kerr nonlinear coefficient, λ_0 is the resonance wavelength, Q_{ext} is the external Quality Factor and Q_{in} is the intrinsic Quality factor.

4.2 Set up for Comb Generation

In this section we are going to discuss the comb generation set up as shown in Fig. 4.4:

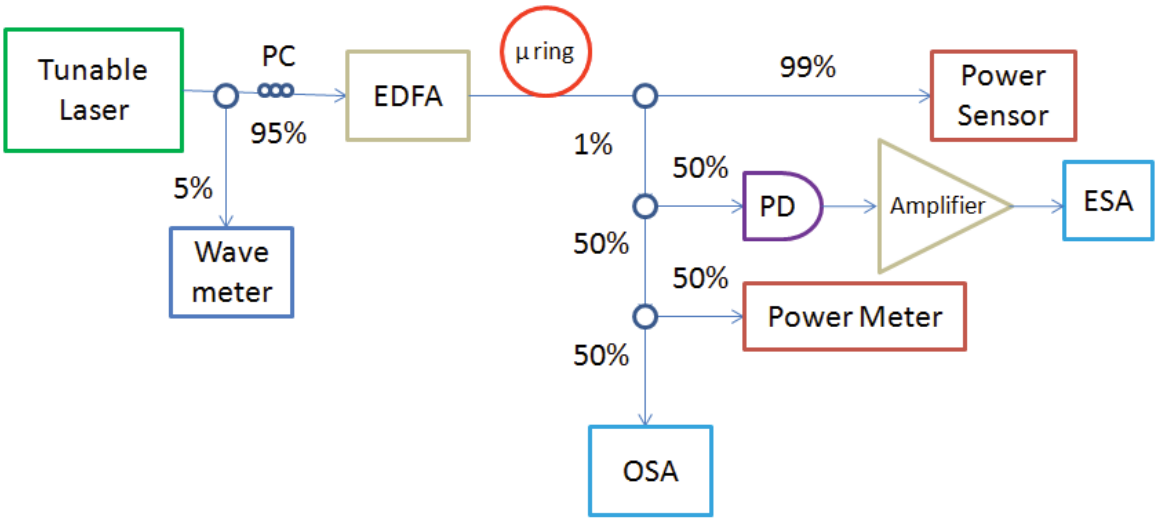

Fig. 4.4. The set up for comb generation. PC=Polarization Controller, PD=Photo-Diode, EDFA= Erbium Doped Fiber Amplifier, OSA=Optical Spectrum Analyzer, ESA= Electrical Spectrum Analyzer, All the blue circles in the figure represents optical splitters with different splitting ratios as shown in their corresponding branches.

In this set up we use a tunable laser source which can be any tunable laser source. In our lab we usually use New Focus laser as the tunable laser source for comb generation. Sometimes we can use the Agilent 8164 laser too, but the tunability of New Focus laser is much better than the Agilent laser. In the New Focus laser there is

piezo control by which we can tune the wavelengths very precisely and reach the resonance for comb generation. For precise measurement of wavelength, we split the output of the tunable laser and send it to a wavelength meter. Thus we can precisely measure the input wavelengths which is crucial for comb generation. After properly optimizing the polarization, we send it to a Erbium Doped Fiber Amplifier (EDFA) to boost the power to reach the comb threshold as shown in equation (4.3).

We couple the microring resonator in our 5 axis stages via a tapered lens fiber. The output of the chip goes through several optical coupler which splits the power into different ratios. The first one splits it into 99/1 ratio and 99% goes to a power sensor by which we can essentially measure almost the whole power that is in the output bus waveguide. As this power might be large, we use ThorLabs S145c sensor can sense up to 3W of power as mentioned in section 2.2. The rest 1% goes to another coupler which splits it into 50-50, the first 50% goes to the ESA for RF noise measurement via a photo-diode and an electric amplifier. The second 50% goes to another coupler which splits it into further 50-50. One of them goes to the OSA for observation of comb spectrum, the other one goes to a power meter which shows us how much power is going to OSA.

5. EXPERIMENTAL RESULTS

In this chapter, we will show all the measured data for one of our designed chips. We have measured a lot chips following the procedure we described in chapter 2-4, but not all of the chips gave us sufficient quality factor for comb generation. So in this thesis, we are going to show one of those chips which actually could produce some frequency comb. We are actually trying to show that we can measure all those important parameters following the procedures that we described in the above mentioned chapters. So, this chapter mainly contains all experimental data and some comparison with our simulated results. In section 5.1, we will show the layout of the structure and give all the design parameters that was needed for fabrication. In section 5.2, we will show the results of transmission measurement and Quality Factor calculations for that chip. In section 5.3 we will show the dispersion measurement data. Section 5.4 will cover the results of comb generation. Finally in section 5.5 we will add some simulation results and compare them with our experimental results.

5.1 Chip Layout

A schematic picture of our designed chip is shown in Fig 5.1. From the figure, we see that the designed microring resonator is basically a C-shaped resonator. In our design, we tried to optimize the straight section part to lower the bending loss due to curved sections. Also the length of our design chosen so that we can reach close to 50 GHz FSR. The bus waveguide for the design is a bend waveguide from where light is coupled inside the microring.The gap size between the bus waveguide and microring was varied in several of our previous designs to obtain a suitable gap size which is close to the critical coupling.

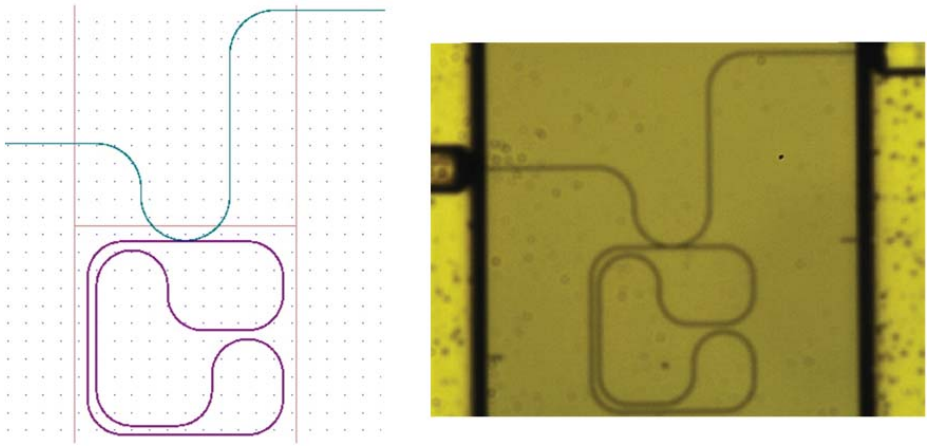

Fig. 5.1. (a)The schematic layout and (b) The microscopic view of the designed C-shaped microring resonator. We have used 2 tapered lens fibers to couple the light to a bent bus waveguide and from there light is coupled to microring resonator.

Also, in some of our previous fabrications we have tried to change different design parameters such as width of the microring resonator, length of the resonator to obtain 50 GHz FSR etc. All the design parameters for the chip are shown in table 5.1.

Table 5.1
Design Parameters For Channel 12 of ND03042016 Chip

Parameter	**Value**
Length (Perimeter)	2887 μm
Width of microring (W)	2 μm
Width of Bus waveguide (B)	1 μm
Bending of bus waveguide	100 μm
Height	740 nm
Gap size (Between Bus waveguide and microring)	300 nm

5.2 Transmission Spectrum and Q-Factor Measurements

The transmission spectrum was measured using the set up shown in Fig. 2.2. The first part was to measure fiber to fiber insertion loss without the chip. The amount of insertion loss that we found was around 3.5 dB. After that we coupled the chip using our 5 axis stage and the tapered lens fibers. Unfortunately we had some problems in the fabrication that there was some gap at the through port end, for which the coupling efficiency was not that high as we usually get. In most of our chips that was fabricated before, we found that the insertion loss after inserting the chip is around 5$\sim$6 dB. But in this case we found the insertion loss is around 10-12 dB. We were able to get few good quality factors from this channel. That is the reason we could generate combs even with this insertion loss.

We used Agilent 81680 for measuring the transmission spectrum of the chip. The sensor HP81632A was used to measure the output power from the microresonator. The transmission spectrum for the chip was taken for two different polarization. At first, we tried to maximize the output power by changing the polarization using polarization controller. The transmission Spectrum corresponds to maximum power is considered as polarization 1 throughout this thesis. In the next attempt, we tried to minimize the output power by changing the polarization controller again. The other polarization, which gives us the minimum power is considered as Polarization 2 throughout in this thesis.

After that we used our MATLAB code to measure the transmission spectrum. Our lab has one computer that is connected to the Agilent laser driver via GPIB and we can control that laser using that MATLAB code. After properly optimizing the polarization we sweep the laser for 60 nm (1520 nm - 1580 nm) and get the transmission spectrum. The transmission spectrum for both the polarization is shown in Fig 5.2:

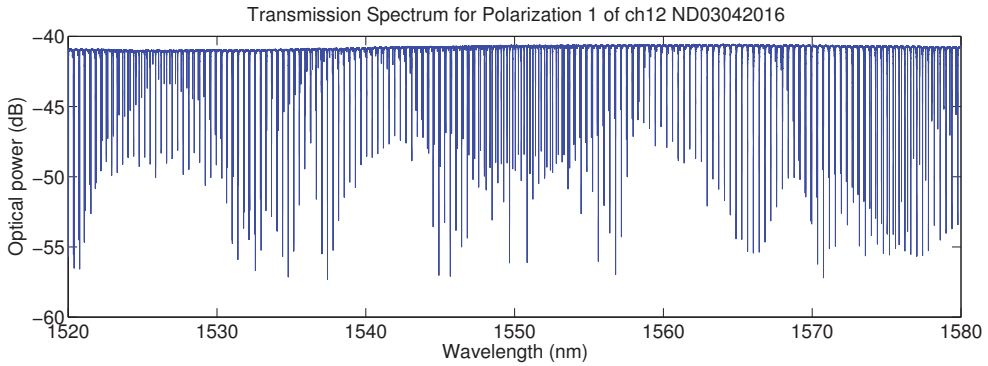

(a) Transmission Spectrum for Polarization 1

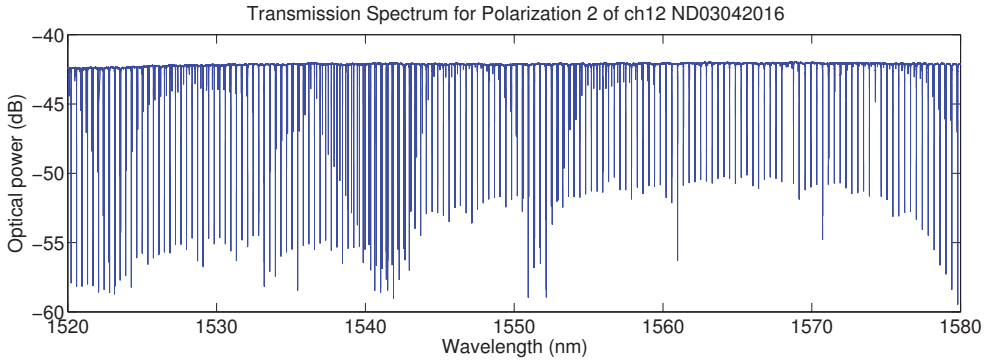

(b) Transmission Spectrum for Polarization 2

Fig. 5.2. The measured Transmission Spectrum for polarization 1 and Polarization 2 for the designed chip, which is channel 12 of the chip titled ND03042016.

From Fig. 5.2, we see that we are getting a very good Extinction Ratio for the channel. In some the resonances the extinction ratio is around ∼15 dB, which is pretty good and probably would mean that we are very close to critical coupling. The reason for such claim is that if we compare the other channel's Extinction Ratio of the same chip (which are not shown in this thesis), this is probably the highest. Now, we can normalize the output optical power to show the plots in terms of transmittance which ranges from 0 to 1. The normalized transmission plots for both the polarization are shown in Fig. 5.3:

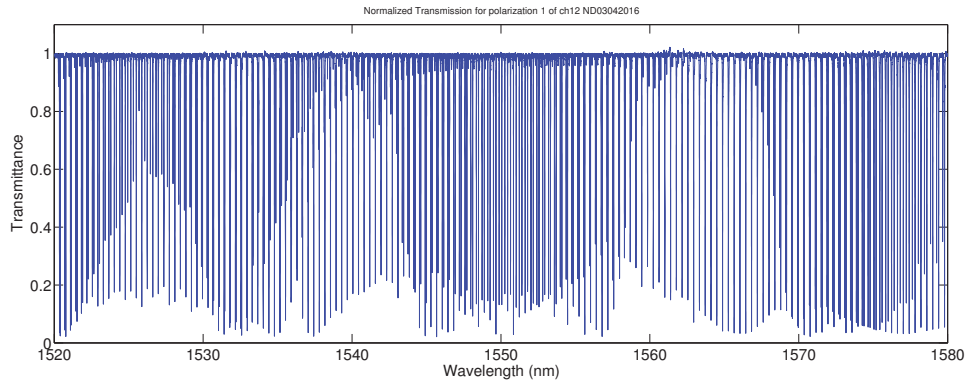

(a) Normalized Transmission Spectrum for Polarization 1

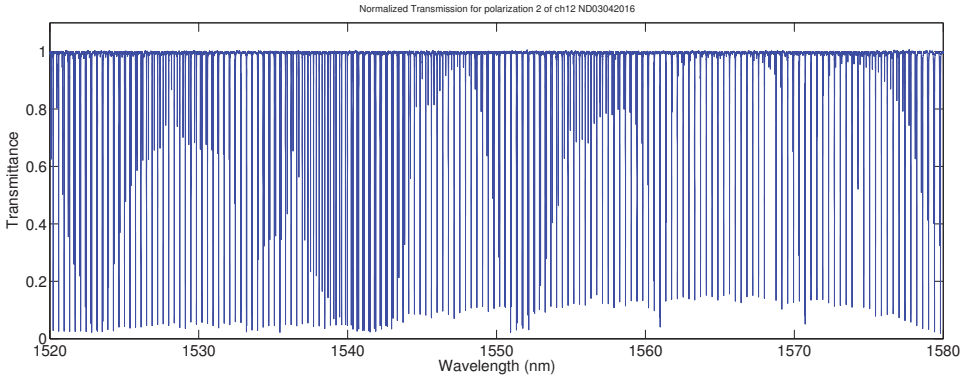

(b) Normalized Transmission Spectrum for Polarization 2

Fig. 5.3. The Normalized Transmission Spectrum for polarization 1 and Polarization 2 for the designed chip, which is channel 12 of the chip titled ND03042016.

From the transmission spectrum we got total 3 modes in this channel. The FSRs for the modes are 49.56 GHz for high Q mode, 48.8 GHz and 47.7 GHz for the other modes around 1550 nm respectively.

The Quality Factors were measured by curve fitting the transmittance as mentioned in section 2.3. We fitted the transmission curve with the equation described in equation (2.21). It is notable that for our calculation of Q, we actually set some threshold for Extinction Ratio. Only the resonances with more than 3 dB extinction

ratio are counted. The reason for that is we have found from our previous experience that comb generation is very very difficult from resonances with less than 3 dB extinction ratio. For this chip we got some good quality factors for polarization 2. The intrinsic and loaded quality factors for all the resonances are shown in Fig. 5.4. Some of the good Quality Factors are also shown in table 5.1 along with some of the fitted curves in Fig. 5.5:

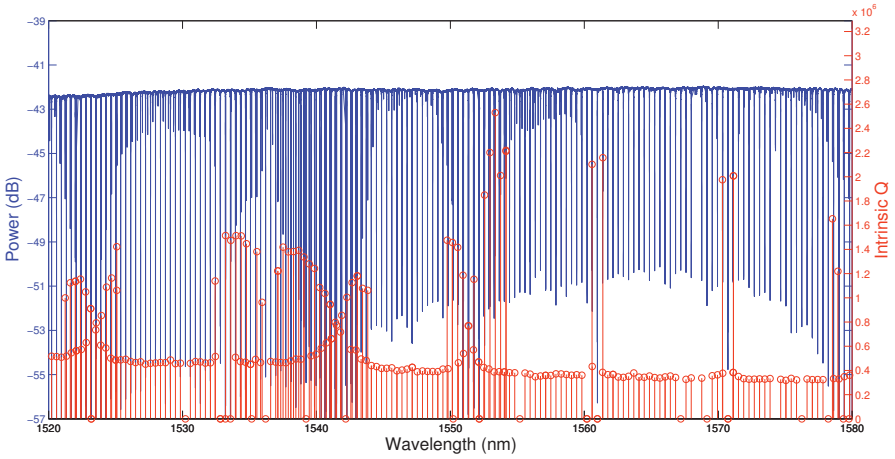

(a) Intrinsic Quality Factors

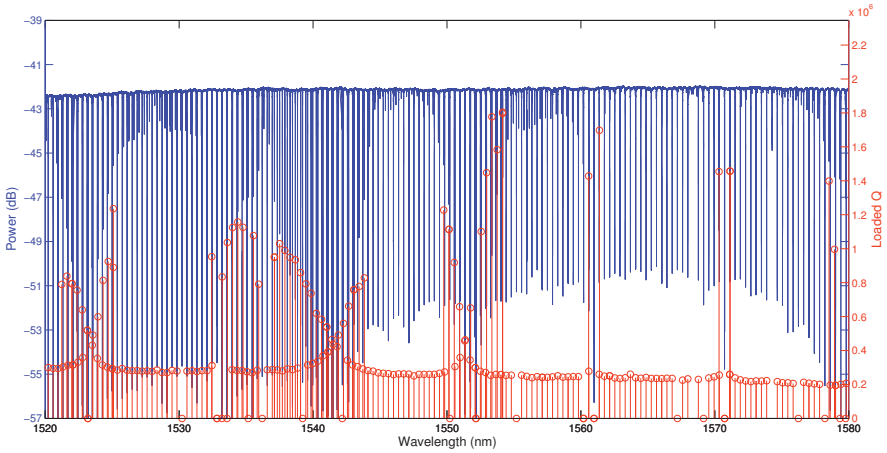

(b) Loaded Quality Factors

Fig. 5.4. The Intrinsic and Loaded Quality Factors along with the transmission spectrum for Polarization 2 of channel 12 of the designed chip titled ND03042016.

Table 5.2
Quality Factors For Channel 12 of ND03042016 Chip

Wavelength (nm)	**Intrinsic Q (Millions)**	**Loaded Q (Millions)**	**Extinction Ratio (dB)**
1553.3562	2.536	1.78	7.4
1554.1546	2.22	1.80	4.0
1552.9575	2.20	1.45	9.7
1561.3881	2.16	1.70	4.5
1560.5788	2.10	1.43	8.0
1553.7552	2.01	1.58	4.6
1571.1398	2.01	1.46	6.7
1570.3202	1.98	1.45	6.3

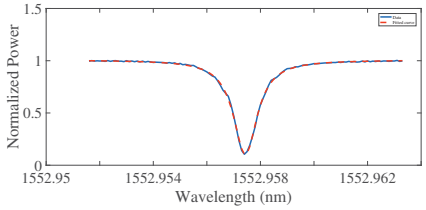

(a) Curve fitting at λ=1552.9575 nm

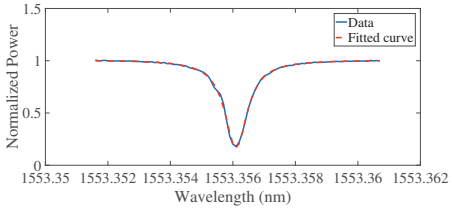

(b) Curve fitting at λ=1553.3562 nm

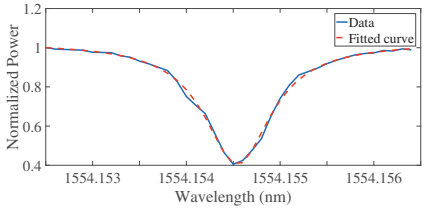

(c) Curve fitting at λ=1554.1546 nm

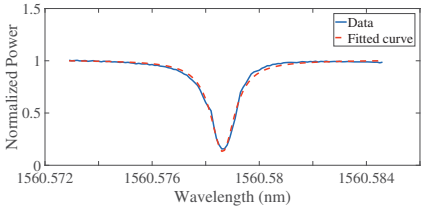

(d) Curve fitting at λ=1560.5788 nm

Fig. 5.5. Fitted curve for calculating quality factors of few resonances. These figure shows that our curve fitting was pretty accurate, thus the calculated quality factors are pretty close to their actual values.

5.3 Dispersion Measurement

We measured the dispersion of the chip following the procedure and the set up described in section 3.4. We gathered data from Oscilloscope using our MATLAB code and then we measured dispersion using the algorithm described in section 3.4.2. There were 3 modes from the transmission spectrum and we calculated dispersion for all the modes by doing linear fit of the FSR evolution as mentioned in section 3.3. Using the coefficients from linear fitting and all other parameters needed we calculated dispersion using equation (3.21). The FSR plot with linear fit is shown in Fig. 5.6, Fig. 5.7 and Fig. 5.8 for mode 1, mode 2 and mode 3 respectively:

During the dispersion measurement, we can match the polarization with the transmission spectrum by tuning the polarization controller in our set up to get the same mode families. Again, we were able to extract the FSR for the modes from the FSR

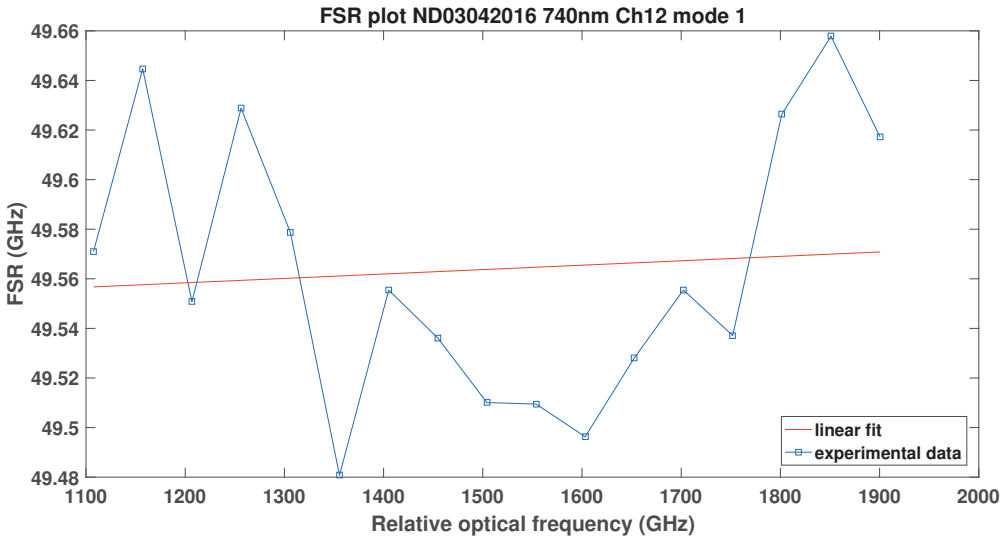

Fig. 5.6. Linear fitting for calculating Dispersion from FSR evolution for high Q mode. The calculated dispersion is around 273 ps/nm-km.

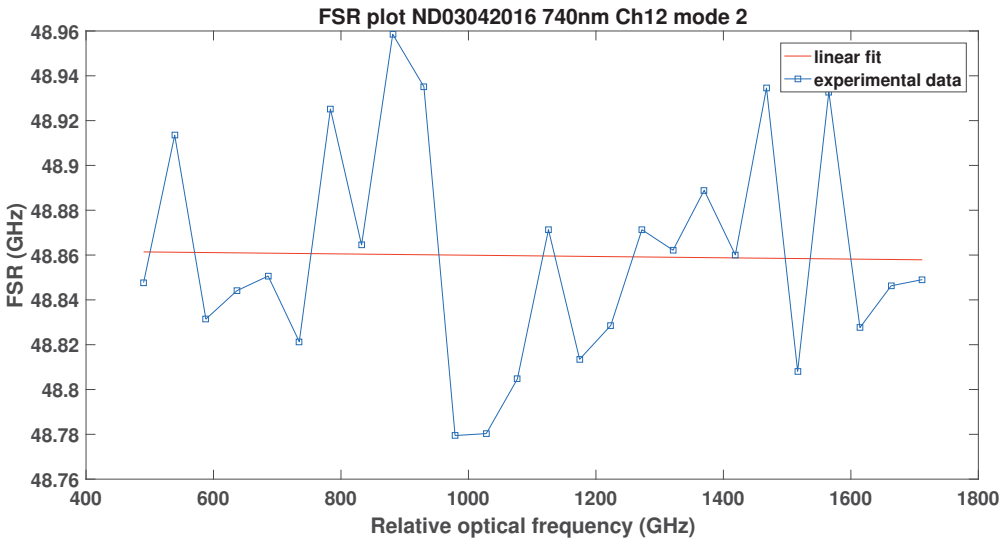

Fig. 5.7. Linear fitting for calculating Dispersion from FSR evolution for mode 2. The calculated dispersion is around -53 ps/nm-km.

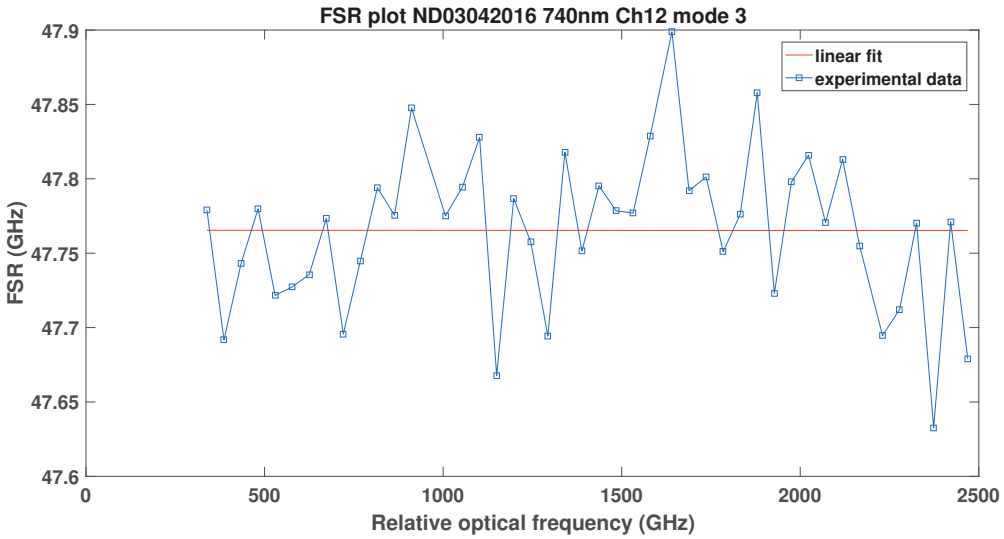

Fig. 5.8. Linear fitting for calculating Dispersion from FSR evolution for mode 3. The calculated dispersion is around -2 ps/nm-km.

evolution plot and the FSRs are very close to the ones we measured from transmission spectrum. All the dispersion measurement data for the chip are shown in Table 5.3:

Table 5.3
Dispersion Measurement Data

Mode number	**FSR (GHz)**	**Dispersion Co-efficient, D (in ps/nm-km)**
1	49.56	273
2	48.86	-53
3	47.75	-2

5.4 Comb Generation

After getting the Quality factors transmission spectrum as shown in table 5.2, we tried to generate some frequency comb from some of those resonances. For comb generation, we actually wanted some resonances between 1540 nm-1560 nm because in this range our EDFA works well. We found several resonances that gave us good quality factors in this range along with some good extinction ratio. We were able to generate frequency combs from a few resonances, but the frequency combs were multiple FSRs away and comb spectrum wasn't that good. But from the resonance at 1552.9575 nm, which has a moderately good quality factor (2.20 million intrinsic Q and 1.45 million loaded Q) and good extinction ratio (around 9.7 dB), we were able to generate single FSR comb with 2W power from EDFA. The OSA spectrum and zoomed in version of the frequency comb that we generated from the resonance at 1552.9575 nm are shown in Fig 5.9:

This comb was type 2 comb because initially the comb lines were spaced multiple FSRs away. And when we cranked up the power more comb lines filled in the middle

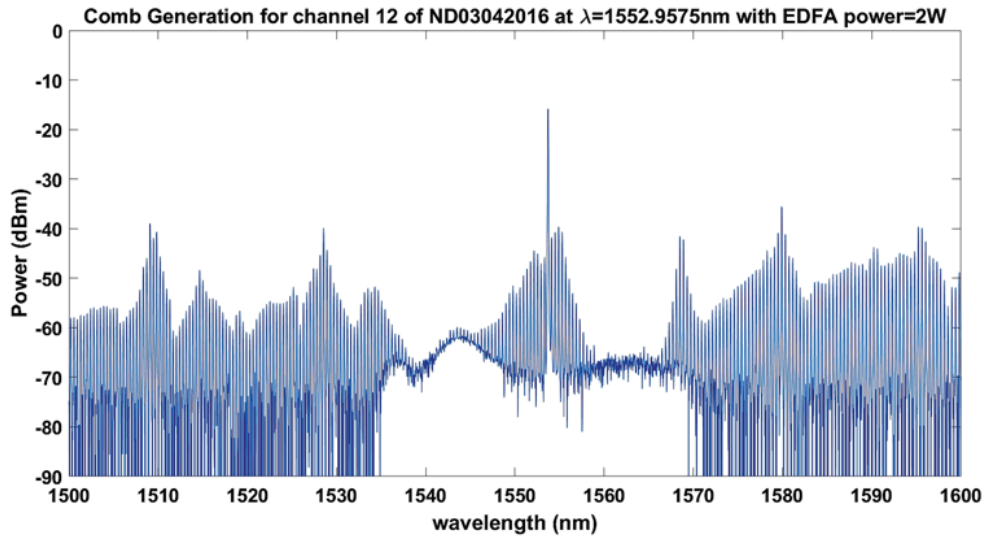

(a) OSA spectrum of Single FSR frequency comb

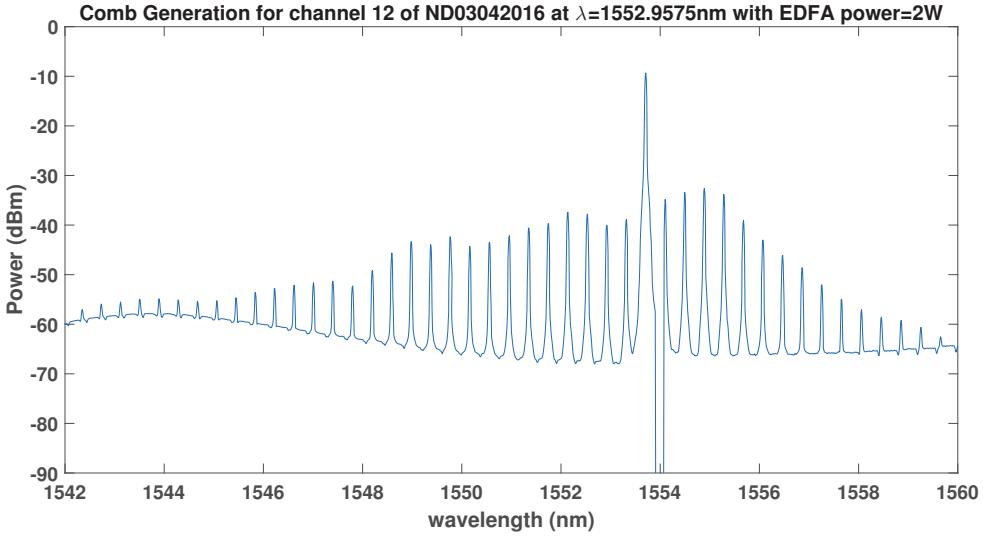

(b) Zoomed in spectrum for the generated comb

Fig. 5.9. Optical frequency comb generated from channel 12 of the chip ND03042016 at λ=1552.9575 nm. The first figure shows the OSA spectrum of the frequency comb and the second figure shows a zoomed in view of the spectrum.

and produced single FSR frequency comb. Also we could see the comb extends for a long span of wavelength, so it has broadband nature. But from the ESA spectrum,

we didn't get any noise, which may be due to the fact that the noise is actually out of the detection level for the current set up. The ESA spectrum for the comb is shown in Fig. 5.10.

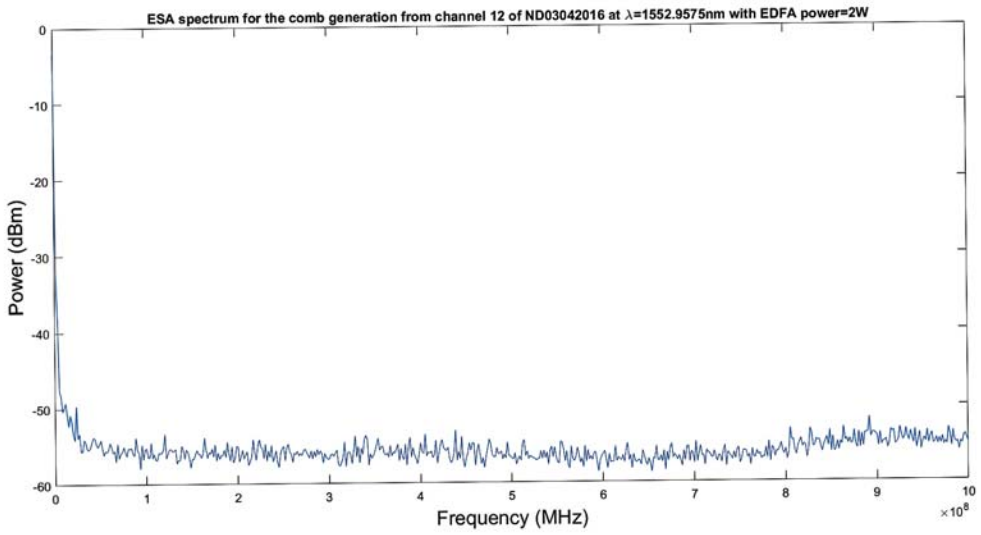

Fig. 5.10. ESA spectrum for the generated frequency comb. ESA doesn't show any intensity noise for the generated comb.

The threshold for comb generation at this resonance can be calculated from equation (4.3). Considering Q_L=1.45e6, Q_i=2.2e6, n_2=2.4e-19 m^2/W, A_{eff}=2e-12 m^2, n_g=2.1,λ=1550e-9 m, R=460e-6 m, we get the threshold value for the comb generation around 75 mW. From experiments, we could generate comb with power at bus waveguide roughly around 80 mW which is close to the value we obtain from the formula.

We could generate comb from other resonances too, but they were type 2 comb too and probably not coherent. One of the example is shown in Fig. 5.11. An important thing to mention here is that we actually don't get much information about the coherence of the generated frequency comb for this comb from this set up. Despite our ESA shows no noise, there might still be some noise below ESA's detection

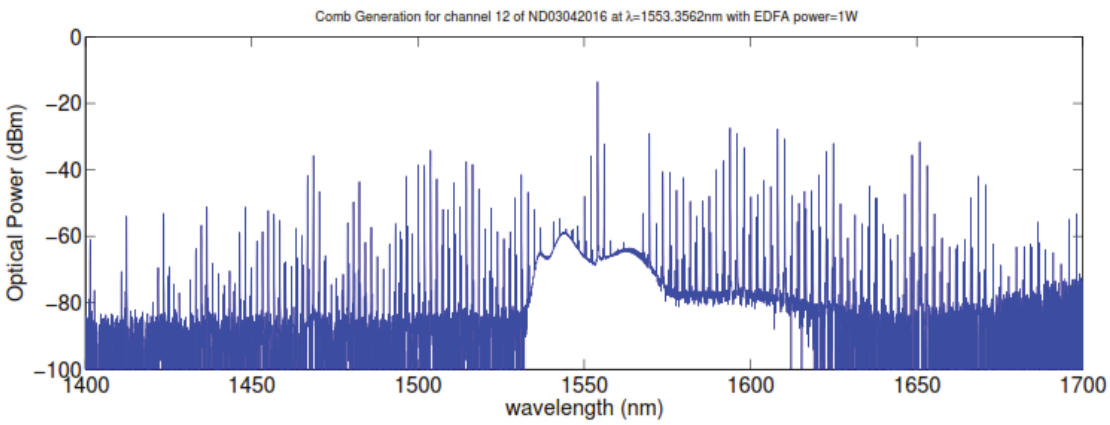

Fig. 5.11. OSA spectrum of the frequency comb generated at 1553.3562 nm.

method. So We can use a fast photo-diode, which can measure beat notes up to 50 GHz, which can be another way to check the presence of noise for the comb that we generated. But a better way to directly check the coherence of the generated frequency combs is the auto-correlation measurement, which is a time domain measurement not mentioned in this thesis. In our lab, we actually do the auto-correlation measurement after generating frequency comb.

5.5 Simulated Results and Comparisons

In this section, we will show some of our simulation results. We actually simulated a couple of things for this design. The first thing is we tried to calculated the effective refractive index for the chips from some previous data and we tried to measure dispersion from that. We have used some of our previous fabrication data for effective refractive index of Silicon Nitride and the Silicon Dioxide at different wavelengths.

For calculating effective refractive index, we used MIT Photonic Bands (MPB) software [44]. We were able to calculate different wave-vectors at different wavelengths

on the basis of our previous fabrication data from where we took the refractive index values for Silicon Nitride and Silicon Dioxide. Each wave vector corresponds to a mode family that our microring waveguide geometry can support. From there, we could easily calculate the effective refractive indexes by:

$$k = \frac{n_{eff}\omega}{c} \tag{5.1}$$

where, k is the wavevector, ω is the angular frequency, c is velocity of light, n_{eff} is the effective refractive index. After calculating effective refractive index, we can calculate the group index by:

$$n_g = n_{eff} - \lambda \frac{dn_{eff}}{d\lambda} \tag{5.2}$$

Figure 5.12 shows us the effective refractive index vs wavelength plot, from where we calculated our group indexes for each mode.

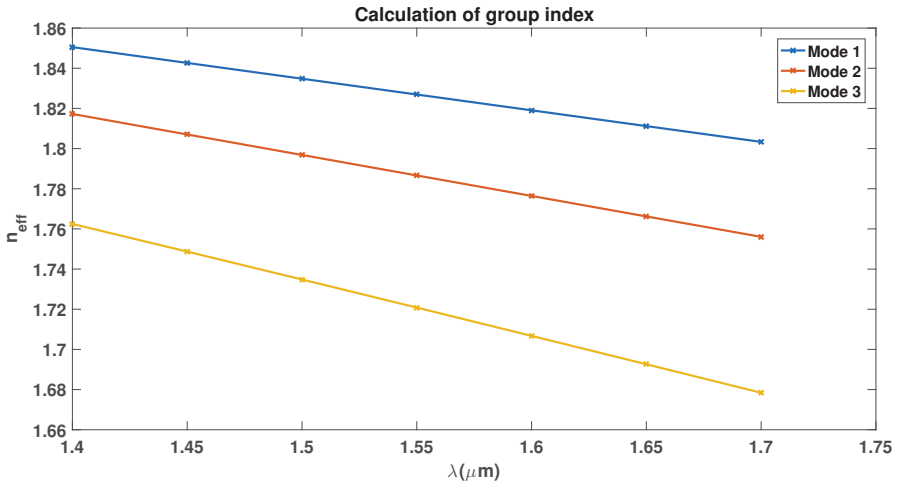

Fig. 5.12. Effective refractive index of Silicon Nitride vs Wavelength plot using the wave vectors obtained from MPB simulation. Each line corresponds to a mode family. From this data using equation (5.2), we calculated the group index for each mode.

We can calculate group index from experimental transmission measurement data using equation (2.10):

$$n_g = \frac{c}{FSR * L} \tag{5.3}$$

where, FSR=Free Spectral ranges for each mode, L is the length or perimeter of the microring and c is the velocity of light. A comparison between the simulated group index and experimental group index is shown in table 5.4.

Table 5.4
Simulated and Experimental Group Index Comparison

Mode number	**Simulated** n_g	**Experimental** n_g	% **Error**
1	2.07	2.09	0.96
2	2.103	2.125	1.04
3	2.155	2.17	0.69

We also obtained dispersion co-efficient D for all the mode families using equation (3.8). After getting group index using MATLAB, we calculated dispersion associated with each mode family. A comparison between simulated and experimental dispersion data is shown in table 5.5:

So we see that our simulated and experimental values are very close. In case of group index calculation our %error is less than 1% for mode 1 and 3 and dispersion coefficients are not too far away. One possible reason for these differences is that we have used some previous fabrication data for simulation. So for the current fabrication the refractive indices for Silicon Nitride and Silicon Dioxide at different wavelengths might not be the same. Again, the high Q resonance only comes up in certain areas in transmission spectrum as shown in Fig. 5.13, it doesn't exist in the whole spectrum. Also, there are some mode interactions with the low Q mode as different regions,

Table 5.5
Comparison Between Simulated and Experimental Dispersion Coefficients

Mode Number	**Simulated Dispersion Coefficient (ps/nm-km)**	**Experimental Dispersion Coefficient (ps/nm-km)**
1	166	273
2	-24	-53
3	-6	-2

which make it very difficult to calculate the value of dispersion in those area. So effectively we have very small amount of points to calculate dispersion for that mode, which may be the reason for the difference. Despite little differences our experimental values are quite close to our simulated results, which validates our measurements.

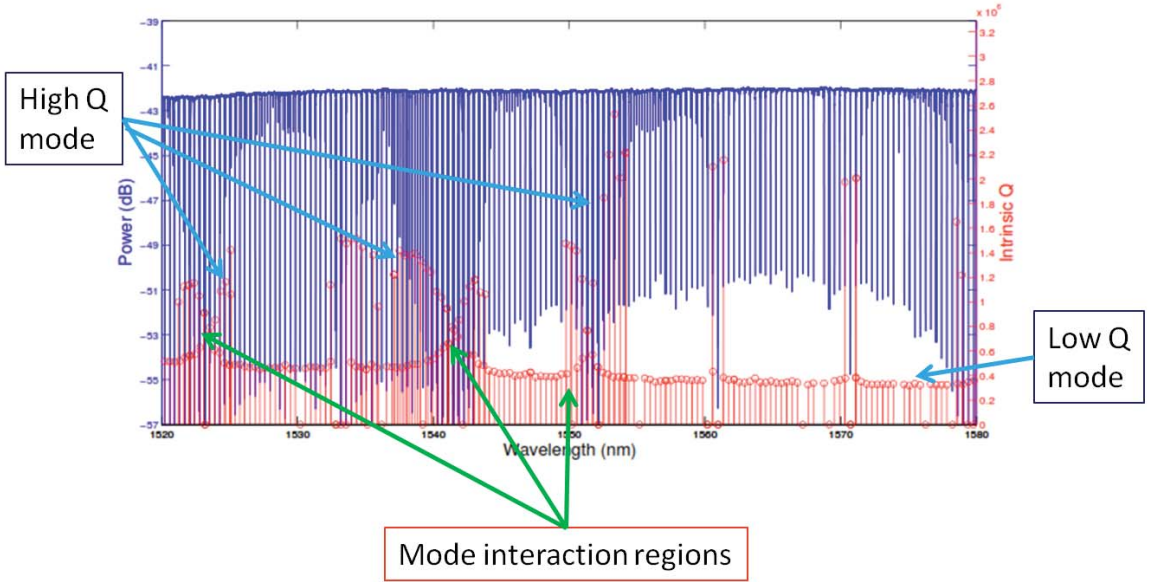

Fig. 5.13. Mode interaction regions between the High Q and Low Q modes

6. SUMMARY AND CONCLUSION

In this thesis, we have tried to describe some of the basic characterization methods for on-chip microring resonators. We showed one of our designed chip and all the characterization results. We have measured transmission spectrum using our described method and measured FSR for all the modes. We measured the quality factors associated with each resonance by curve fitting and showed the intrinsic and loaded Q factors along with the transmission data. It is worth mentioning that we can basically separate the mode families by their quality factors too. Usually modes of the same family maintain the same level of quality factors and we can identify mode crossing areas from those plots as shown in Fig. 5.13. We have reported some of the good quality factors for the chip by showing the almost exact curve fitting for each of them.

We have introduced the modified version of dispersion measurement set up, which has simplified the complexity of acquiring data from dispersion measurement set up and also reduced the chances of error due to overlapping of markers. We have shown the value of dispersion coefficient for all the modes.

We were able to generate some combs from couple of resonances using the method and the set up described in chapter 4. We could generate a type II comb with single FSR spacing following our set up and it was our first few attempts to generate frequency combs at 50 GHz. So we hope to improve the comb generation in future attempts and get broadband coherent single FSR combs.

We simulated with some of our design parameters and material properties used for fabrication. The simulation results are pretty close to the experimental results.

In short, we were able to characterize a Silicon Nitride microring resonator and calculated few important parameters that are necessary for the application of the chip. By following the same methods, we can characterize any chip. So this will be helpful for those who needs to characterize any optical chip. But the set ups and measurements can be further improved. For example, currently we measure FSR by taking several resonances around 1550 nm and take average of FSR of them. But this can be extended for the whole range the mode exists and that could give us a better estimation of FSR. We can use some reference laser to find the FSR accurately as our current FSR measurement is dependent on the transmission measurement. In our lab, we have 2 stages for transmission measurements and the accuracy of measurements are not same in both. But the data obtained by different laser sources gave us pretty much similar data. So it is important that we have a very good tunable laser and very good sensor along with some reference laser to accurately measure our resonant frequencies.

For the quality factor measurement we use transmission data and curve fitting. So again the accuracy of transmission data is important as Quality factor is a very important parameter and it is important that we get an accurate value for it. For high Q devices, we can use the dispersion measurement set ups to accurately locate resonances and find quality factors from the transmission data obtain from that set up, but with low and moderate Quality factors, transmission data is probably enough.

We can do phase measurements to check whether the device is under-coupled or over-coupled. We can use a phase modulator and after generating initial side-bands, we can sweep the RF frequency of the phase modulators to create the beating note between the generated side-band and the resonance. And from that we can get the phase response using a Voltage Network Analyzer (VNA). If the phase response gives us a 2π phase shift, the device is over-coupled and if the phase shift is less that 2π, then the device is under-coupled. The details of this method is described in the

supplementary section of [45]. This phase measurement method can also be used to check the existence of Solitons and find the detuning for comb generation as shown in [46].

After comb generation, it is necessary to check the coherence of the generated comb and that can be done by further time domain measurements using auto-correlation. We can also try with a photo-diode that has larger bandwidth to check the ESA spectrum to check the coherence of the generated combs. The soliton generation is another exciting prospect which is has very good prospect. We can check the Dispersion compensation is another process by which we can check the shape of output from microring resonator. If the output is a soliton, it will be a pure pulse. So there are lot of exciting stuffs that can be explored for complete characterization and improvement of characterization processes.

LIST OF REFERENCES

LIST OF REFERENCES

[1] B. E. Little, S. T. Chu, H. A. Haus, J. Foresi, and J. P. Laine, "Microring resonator channel dropping filters," *Journal of Lightwave Technology*, vol. 15, no. 6, pp. 998–1005, 1997.

[2] T. J. Kippenberg, J. Kalkman, A. Polman, and K. J. Vahala, "Demonstration of an erbium-doped microdisk laser on a silicon chip," *Physical Review A - Atomic, Molecular, and Optical Physics*, vol. 74, p. 051802, nov 2006.

[3] B. Min, T. J. Kippenberg, L. Yang, K. J. Vahala, J. Kalkman, and A. Polman, "Erbium-implanted high-Q silica toroidal microcavity laser on a silicon chip," *Physical Review A - Atomic, Molecular, and Optical Physics*, vol. 70, no. 3, 2004.

[4] M. Cai, O. Painter, K. J. Vahala, and P. C. Sercel, "Fiber-coupled microsphere laser," *Optics Letters*, vol. 25, p. 1430, oct 2000.

[5] A. M. Armani, R. P. Kulkarni, S. E. Fraser, R. C. Flagan, and K. J. Vahala, "Label-free, single-molecule detection with optical microcavities.," *Science*, vol. 317, pp. 783–7, aug 2007.

[6] W. H. P. Pernice, C. Xiong, C. Schuck, and H. X. Tang, "Second harmonic generation in phase matched aluminum nitride waveguides and micro-ring resonators," *Applied Physics Letters*, vol. 100, p. 223501, may 2012.

[7] J. S. Levy, M. A. Foster, A. L. Gaeta, and M. Lipson, "Harmonic generation in silicon nitride ring resonators.," *Optics express*, vol. 19, no. 12, pp. 11415–11421, 2011.

[8] A. A. Savchenkov, A. B. Matsko, M. Mohageg, D. V. Strekalov, and L. Maleki, "Parametric oscillations in a whispering gallery resonator," *Optics Letters*, vol. 32, p. 157, dec 2006.

[9] T. J. Kippenberg, S. M. Spillane, and K. J. Vahala, "Kerr-nonlinearity optical parametric oscillation in an ultrahigh-Q toroid microcavity.," *Physical review letters*, vol. 93, p. 083904, aug 2004.

[10] A. A. Savchenkov, A. B. Matsko, D. Strekalov, M. Mohageg, V. S. Ilchenko, and L. Maleki, "Low threshold optical oscillations in a whispering gallery mode CaF 2 resonator," *Physical Review Letters*, vol. 93, p. 243905, dec 2004.

[11] S. M. Spillane, T. J. Kippenberg, and K. J. Vahala, "Ultralow-threshold Raman laser using a spherical dielectric microcavity.," *Nature*, vol. 415, pp. 621–3, mar 2002.

[12] B. Min, T. J. Kippenberg, and K. J. Vahala, "Compact, fiber-compatible, cascaded Raman laser," *Optics Letters*, vol. 28, p. 1507, sep 2003.

[13] T. J. Kippenberg, S. M. Spillane, D. K. Armani, and K. J. Vahala, "Ultralow-threshold microcavity Raman laser on a microelectronic chip," *Optics Letters*, vol. 29, p. 1224, jun 2004.

[14] I. S. Grudinin and L. Maleki, "Ultralow-threshold Raman lasing with CaF_2 resonators," *Optics Letters*, vol. 32, p. 166, dec 2006.

[15] J. Xie, L. Zhou, Z. Zou, J. Wang, X. Li, and J. Chen, "Continuously tunable reflective-type optical delay lines using microring resonators.," *Optics express*, vol. 22, pp. 817–23, jan 2014.

[16] S.-H. Hsu, Y.-C. Yang, Y.-H. Su, S.-M. Wang, S.-A. Huang, and C.-Y. Lin, "Biosensing using microring resonator interferograms.," *Sensors (Basel, Switzerland)*, vol. 14, pp. 1184–94, jan 2013.

[17] Y. Liu, Y. Xuan, X. Xue, P.-H. Wang, S. Chen, A. J. Metcalf, J. Wang, D. E. Leaird, M. Qi, and A. M. Weiner, "Investigation of mode coupling in normal-dispersion silicon nitride microresonators for Kerr frequency comb generation," *Optica*, vol. 1, p. 137, aug 2014.

[18] P. Del'Haye, A. Schliesser, O. Arcizet, T. Wilken, R. Holzwarth, and T. J. Kippenberg, "Optical frequency comb generation from a monolithic microresonator.," *Nature*, vol. 450, pp. 1214–7, dec 2007.

[19] T. Herr, *Solitons and dynamics of frequency comb formation in optical microresonators*. PhD thesis, EPFL (Lausanne), 2013.

[20] D. J. Moss, R. Morandotti, A. L. Gaeta, and M. Lipson, "New CMOS-compatible platforms based on silicon nitride and Hydex for nonlinear optics," *Nature Photonics*, vol. 7, pp. 597–607, jul 2013.

[21] H. Haus, W. Huang, S. Kawakami, and N. Whitaker, "Coupled-mode theory of optical waveguides," *Journal of Lightwave Technology*, vol. 5, no. 1, pp. 16–23, 1987.

[22] D. H. Geuzebroek and A. Driessen, *Wavelength Filters in Fibre Optics*, ch. Ring-Resonator-Based Wavelength Filters, pp. 341–379. Berlin, Heidelberg: Springer Berlin Heidelberg, 2006.

[23] W. Bogaerts, P. De Heyn, T. Van Vaerenbergh, K. De Vos, S. Kumar Selvaraja, T. Claes, P. Dumon, P. Bienstman, D. Van Thourhout, and R. Baets, "Silicon microring resonators," *Laser & Photonics Reviews*, vol. 27, no. 1, pp. 47–73, 2011.

[24] P. Del'Haye, *Optical Frequency Comb Generation in Monolithic Microresonators*. PhD thesis, Ludwig Maximilian University of Munich, 2011.

[25] S. Xiao, M. H. Khan, H. Shen, and M. Qi, "Modeling and measurement of losses in silicon-on-insulator resonators and bends," *Optics Express*, vol. 15, p. 10553, aug 2007.

[26] Fahmida Ferdous, *On chip frequency comb: characterization and optical arbitrary waveform generation*. PhD thesis, Purdue University, 2012.

[27] A. M. Weiner, *Ultrafast Optics*. Hoboken, NJ, USA: John Wiley & Sons, Inc., jun 2009.

[28] W. Sellmeier, "Zur Erklärung der abnormen Farbenfolge im Spectrum einiger Substanzen," *Annalen der Physik und Chemie*, no. 219, pp. 272–282, 1871.

[29] M. J. Weber, *Handbook of Optical Materials*. CRC Press, 2003.

[30] P. Del'Haye, O. Arcizet, M. L. Gorodetsky, R. Holzwarth, and T. J. Kippenberg, "Frequency comb assisted diode laser spectroscopy for measurement of microcavity dispersion," *Nature Photonics*, vol. 3, pp. 529–533, aug 2009.

[31] S. Chen, "Dispersion measurement for on-chip microresonator," Master's thesis, Purdue University, 2015.

[32] Newport Corporation, "http://www.newport.com/Velocity-Widely-Tunable-Lasers/991179/1033/info.aspx."

[33] Rohde&SchwarzInc., "https://www.rohde-schwarz.com/us/product/rto1000-productstartpage_63493-191808.html."

[34] T. J. Kippenberg, R. Holzwarth, and S. A. Diddams, "Microresonator-based optical frequency combs.," *Science (New York, N.Y.)*, vol. 332, pp. 555–9, apr 2011.

[35] S. A. Diddams, L. Hollberg, and V. Mbele, "Molecular fingerprinting with the resolved modes of a femtosecond laser frequency comb.," *Nature*, vol. 445, pp. 627–30, feb 2007.

[36] T. Steinmetz, T. Wilken, C. Araujo-Hauck, R. Holzwarth, T. W. Hänsch, L. Pasquini, A. Manescau, S. D'Odorico, M. T. Murphy, T. Kentischer, W. Schmidt, and T. Udem, "Laser frequency combs for astronomical observations.," *Science (New York, N.Y.)*, vol. 321, pp. 1335–7, sep 2008.

[37] F. Ferdous, H. Miao, D. E. Leaird, K. Srinivasan, J. Wang, L. Chen, L. T. Varghese, and A. M. Weiner, "Spectral line-by-line pulse shaping of on-chip microresonator frequency combs," *Nature Photonics*, vol. 5, pp. 770–776, oct 2011.

[38] A. Kordts, M. Pfeiffer, H. Guo, V. Brasch, and T. J. Kippenberg, "Higher order mode suppression in high-Q anomalous dispersion SiN microresonators for temporal dissipative Kerr soliton formation," *Optics letters*, vol. 41, no. 3, pp. 452–455, 2015.

[39] A. R. Johnson, Y. Okawachi, J. S. Levy, J. Cardenas, K. Saha, M. Lipson, and A. L. Gaeta, "Chip-based frequency combs with sub-100 ghz repetition rates," *Opt. Lett.*, vol. 37, pp. 875–877, Mar 2012.

[40] T. Herr, K. Hartinger, J. Riemensberger, C. Y. Wang, E. Gavartin, R. Holzwarth, M. L. Gorodetsky, and T. J. Kippenberg, "Universal formation dynamics and noise of Kerr-frequency combs in microresonators," *Nature Photonics*, vol. 6, pp. 480–487, jun 2012.

[41] F. Ferdous, H. Miao, P.-H. Wang, D. E. Leaird, K. Srinivasan, L. Chen, V. Aksyuk, and A. M. Weiner, "Probing coherence in microcavity frequency combs via optical pulse shaping.," *Optics express*, vol. 20, pp. 21033–43, sep 2012.

[42] P.-H. Wang, F. Ferdous, H. Miao, J. Wang, D. E. Leaird, K. Srinivasan, L. Chen, V. Aksyuk, and A. M. Weiner, "Observation of correlation between route to formation, coherence, noise, and communication performance of Kerr combs.," *Optics express*, vol. 20, pp. 29284–95, dec 2012.

[43] A. Matsko, *Practical Applications of Microresonators in Optics and Photonics*, vol. 146 of *Optical Science and Engineering*. CRC Press, mar 2010.

[44] S. G. Johnson and J. D. Joannopoulos, "Block-iterative frequency-domain methods for maxwell's equations in a planewave basis," *Opt. Express*, vol. 8, no. 3, pp. 173–190, 2001.

[45] X. Xue, Y. Xuan, Y. Liu, P.-H. Wang, S. Chen, J. Wang, D. E. Leaird, M. Qi, and A. M. Weiner, "Mode-locked dark pulse Kerr combs in normal-dispersion microresonators," *Nature Photonics*, vol. 9, pp. 594–600, aug 2015.

[46] M. Karpov, H. Guo, E. Lucas, A. Kordts, M. H. P. Pfeiffer, G. Lihachev, V. E. Lobanov, M. L. Gorodetsky, and T. J. Kippenberg, "Universal dynamics and controlled switching of dissipative Kerr solitons in optical microresonators," 2016.